

AD-A119 369

WASHINGTON STATE UNIV PULLMAN DEPT OF PHYSICS  
GLORY AND RAINBOW ENHANCED ACOUSTIC BACKSCATTERING FROM FLUID S--ETC(U)

F/G 20/1

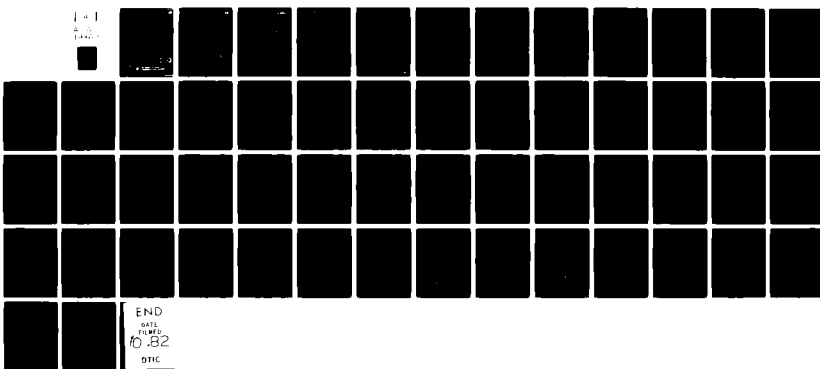
SEP 82 P L MARSTON, D S LANGLEY

N00014-80-C-0838

NL

UNCLASSIFIED

TR-2



END  
DATE  
10-18-82  
BTIC

AD A119369

DTIC FILE COPY



DEPARTMENT OF PHYSICS  
WASHINGTON STATE UNIVERSITY

DISTRIBUTION STATEMENT A

Approved for public release;  
Distribution Unlimited

DTIC  
SELECTED  
SEP 20 1982  
S H

82 09 20 010

DEPARTMENT OF PHYSICS  
WASHINGTON STATE UNIVERSITY  
PULLMAN, WA 99164-2814

DP

TECHNICAL REPORT NO. 2

GLORY AND RAINBOW ENHANCED ACOUSTIC  
BACKSCATTERING FROM FLUID SPHERES: MODELS  
FOR DIFFRACTED AXIAL FOCUSING

by

Philip L. Marston and Dean S. Langley

September 1, 1982

Prepared for:  
OFFICE OF NAVAL RESEARCH  
CONTRACT NO. N00014-80-C-0838

DTIC  
ELECTED  
SEP 20 1982  
S H

Approved for public release; distribution unlimited  
Reproduction in whole or in part is permitted for  
any purpose of the United States Government

Unclassified

SECURITY CLASSIFICATION OF THIS PAGE (When Data Entered)

REPORT DOCUMENTATION PAGE		READ INSTRUCTIONS BEFORE COMPLETING FORM
1. REPORT NUMBER 2	2. GOVT ACCESSION NO. A119369	3. RECIPIENT'S CATALOG NUMBER
4. TITLE (and Subtitle) GLORY AND RAINBOW ENHANCED ACOUSTIC BACKSCATTERING FROM FLUID SPHERES: MODELS FOR DIFFRACTED AXIAL FOCUSING		5. TYPE OF REPORT & PERIOD COVERED Interim Technical Report 1 July 81 - 31 August 82
7. AUTHOR(s) Philip L. Marston and Dean S. Langley		6. PERFORMING ORG. REPORT NUMBER N00014-80-C-0838
9. PERFORMING ORGANIZATION NAME AND ADDRESS Department of Physics Washington State University Pullman, WA 99164-2814		10. PROGRAM ELEMENT, PROJECT, TASK AREA & WORK UNIT NUMBERS
11. CONTROLLING OFFICE NAME AND ADDRESS Office of Naval Research Physics Division Office Arlington, VA 22217		12. REPORT DATE 1 September 1982
14. MONITORING AGENCY NAME & ADDRESS (if different from Controlling Office)		13. NUMBER OF PAGES 51 + iv
		15. SECURITY CLASS. (of this report) Unclassified
		15a. DECLASSIFICATION/DOWNGRADING SCHEDULE
16. DISTRIBUTION STATEMENT (of this Report)  Approved for public release; distribution unlimited		
17. DISTRIBUTION STATEMENT (of the abstract entered in Block 20, if different from Report)		
18. SUPPLEMENTARY NOTES Submitted for publication to the <u>Journal of the Acoustical Society of America</u> .		
19. KEY WORDS (Continue on reverse side if necessary and identify by block number) Acoustic scattering, Inverse scattering, Elastic-wave scattering, Backscattering, Sonar calibration, Physical acoustics, Underwater acoustics ultrasonics		
20. ABSTRACT (Continue on reverse side if necessary and identify by block number) Transmitted-wave contributions to backscattering from large fluid spheres are calculated. Amplitudes due to glory rays are enhanced, relative to those of axial reflections, because of focusing. The glory pressure amplitudes are proportional to $a^2(ka)^{1/2}$ where $a$ is the sphere's radius and $k$ is the wavenumber. The model, though similar in form to one for optical		

Unclassified

SECURITY CLASSIFICATION OF THIS PAGE (When Data Entered)

scattering from air bubbles [D. S. Langley and P. L. Marston, Phys. Rev. Lett. 47, 913-916 (1981)], contains new features to facilitate the summing of amplitudes in a range of angles. An additional enhancement due to rainbow focusing is modeled for certain sound velocity ratios  $M$ ; for these  $M$  the backscattered amplitude is proportional to  $a_u^2(ka)^{2/3}$ . Major features of the exact scattering are reproduced by these models when  $ka = 1000$  and (with defects)  $ka = 100$ . The enhancements are not intrinsically due to resonance. Applications to the design of passive sonar targets are noted.

## TABLE OF CONTENTS

	Page
<b>TITLE PAGE . . . . .</b>	<b>1</b>
<b>REPORT DOCUMENTATION PAGE . . . . .</b>	<b>11</b>
<b>INTRODUCTION . . . . .</b>	<b>1</b>
<b>SECTION NO.</b>	
<b>I. Ray Acoustics and Axial Focusing . . . . .</b>	<b>2</b>
<b>II. Amplitude and Phase in the Exit Plane . . . . .</b>	<b>6</b>
<b>III. Diffraction and the Far-Field Scattering Amplitude . . . . .</b>	<b>9</b>
<b>IV. Discussion of Model and Comparison with Exact Scattering from Spheres with <math>M &lt; 1</math> . . . . .</b>	<b>16</b>
<b>V. Spheres with <math>M &gt; 1</math> and Combined Rainbow and Glory Scattering . . . . .</b>	<b>19</b>
<b>VI. Applications to Underwater Acoustics . . . . .</b>	<b>23</b>
<b>Acknowledgments . . . . .</b>	<b>25</b>
<b>APPENDIX</b>	
<b>A. Curvature and Spreading of Glory Wavefronts . . . . .</b>	<b>25</b>
<b>B. Angle-Dependent Phase Shift Via the Method of Stationary Phase . . .</b>	<b>26</b>
<b>C. Amplitude of the One-Bounce Axial Ray . . . . .</b>	<b>28</b>
<b>References . . . . .</b>	<b>29</b>
<b>Tables . . . . .</b>	<b>33</b>
<b>Figure Captions . . . . .</b>	<b>35</b>
<b>Figures . . . . .</b>	<b>36</b>
<b>Abstract Descriptive of the Scattering Experiment Cited in Reference 11 . . .</b>	<b>49</b>
<b>Report Distribution List . . . . .</b>	<b>50</b>



SEARCHED	INDEXED	FILED	Distribution/ Availability Codes
SERIALIZED	FILED	RECORDED	
APR 1977			A

## INTRODUCTION

The backscattering of light from droplets of water in clouds is known to be enhanced due to a weak focusing in the backward axial direction.<sup>1</sup> This axial focusing gives rise to the optical effect known as the "glory" (Ref. 1-6 and references cited therein). Axial focusing is also known to be present in the classical and quantum mechanical scattering of particles where the enhancement of the differential cross section is known as the<sup>7</sup> "glory effect." Manifestations of this type of focusing in acoustics, though previously noted,<sup>8,9</sup> are relatively unexplored. In the present paper we derive a physical-optics approximation which describes the effects of diffraction on the axial focusing of glory rays in fluid spheres. We verify our approximation by comparing it with numerical computations of the partial-wave sum for the exact scattering from inviscid fluid spheres (formulated e.g. in Ref. 10). It is also shown that the backscattering can be further enhanced by choosing the sound velocity ratio such that glory and rainbow rays coincide.

The paths of rays through a sphere are determined by the acoustic refractive index  $M = c_o/c_i$  where  $c_o$  and  $c_i$  are the sound velocities of the outer and inner fluids, respectively. The incident wave is taken to be a plane wave; it is unmodulated and has a wavelength  $\lambda$  in the outer fluid. A physical-optics approximation for the diffraction limited axial focusing is derived here; the derivation assumes that  $\lambda \ll$  the sphere's radius  $a$ . Comparisons with the exact partial-wave sum, made for several  $M < 1$  with  $ka = 100$  and  $1000$  (where  $k = 2\pi/\gamma$  is the wavenumber of the incident wave), demonstrate the legitimacy of the method. Rays which reflect from the front and rear poles of the sphere (the "axial rays") experience no focusing; consequently their amplitudes are smaller than those of the focused glory rays when  $ka$  is large.

A second paper<sup>11</sup> extends the present results to certain cases of glory scattering of ultrasonic pulses by an elastic sphere in water; it also describes direct observations of diffraction limited backward axial focusing. When rays inside an elastic sphere are not mixed in their type (i.e., they are all shear or all longitudinal rays), the paths are the same as those for a fluid sphere with  $c_1$  taken to be either the shear or the longitudinal wave velocities. Consequently, the paths in fluid spheres with  $M < 1$  most closely resemble those for most elastic spheres. The emphasis of the present paper is on fluid spheres with  $M < 1$ ; however, in Sec. V we model scattering from fluid spheres with  $M > 1$  and present computations of the exact scattering.

The present description of the acoustic glory may also be extended to the case of a spherical elastic shell filled with a liquid. Targets of this type are asserted to be useful as navigational aids and for the calibration of sonar devices. As described in Sec. V, backscattering from a fluid sphere should be quite large when  $M \approx 1.180$ . This enhancement of the scattering, which is due to a coincidence of rainbow and glory rays, should also be applicable to the design of liquid-filled shells with unusually large target strengths. Some applications to shells are noted in Sec. VI.

Our derivation of the scattering amplitude for backward and near backward directions will parallel our previous treatments of the backscattering of light from spherical bubbles<sup>4-6</sup> in liquids and other dielectric spheres.<sup>5</sup> To facilitate a comparison with the exact scattering, we derive, for the first time, the dependence of the phase of the glory scattering on the scattering angle.

### I. Ray Acoustics and Axial Focusing

In this section we review the elementary ray acoustics of a sphere and the geometric effect which gives rise to axial focusing. Ray paths are

described by Snell's law:

$$\sin\theta = M \sin\nu \quad (1)$$

where  $\theta$  is the angle of incidence at the sphere's surface and  $\nu$  is the angle of refraction. The number of chords inside the sphere for a given ray will be denoted by  $n$ . Several rays which are reflected and refracted in the near backward direction are shown in Fig. 1. The deviation  $\gamma$  in the direction of a ray from the backward axis (the CC' axis) is given by

$$\gamma = \theta - \beta, \quad (2)$$

$$\beta = 2n\nu - \theta + (2 - n)\pi, n > 1 \quad (3)$$

where  $\beta$  is the internal angle (relative to the CC' axis) of the point at which a ray leaves the sphere. [Equation (2) may be derived by noting that the direction shifts due to the initial and final refractions have the same magnitude. See Fig. 2.] The roots of  $\gamma = 0$  having  $0 < \theta < \theta_{\max}$  will be denoted by  $\theta_n$  and the associated rays will be referred to as glory rays. Here  $\theta_{\max} = \pi/2$  when  $M > 1$  and  $\theta_{\max} = \theta_c$  when  $M < 1$  where  $\theta_c = \arcsin(M)$  is the critical angle of incidence. Exact backscattering also occurs for rays with  $\theta = 0$  and  $\gamma = (n-2)\pi, n = 0, 2, 4, \dots$ ; these rays will be referred to as axial rays. Certain axial and glory rays are shown as the solid lines in Fig. 1.

The following is a summary of conditions on  $M$  and  $n$  for glory rays to exist. It is well known<sup>1,2</sup> that  $n = 2$  glory rays exist for  $\sqrt{2} < M < 2$ . The emphasis of the present paper will be a class of glory rays which exist for<sup>3</sup>  $0 < M \leq M'_n$  with  $n > 2$ . The upper bounds  $M'_n$  are  $> 1$  with  $M'_n \rightarrow 1$  as  $n \rightarrow \infty$  and  $M'_{n+1} < M'_n$ . We have previously demonstrated that:<sup>3</sup>

$$M'_3 = (3^{1/2} 6 - 9)^{1/2} \approx 1.179960 \quad (4)$$

$$M'_4 = (4/3)(2/3)^{1/2} \approx 1.088662 \quad (5)$$

Most of our discussion will be concerned with spheres with  $M < 1$ .

The general class of glory rays in such spheres is described by  $\theta = \beta'$  where  $\beta' = \beta + n'2\pi$  where  $2n' + 1$  is the number of times rays cross the symmetry axis. It is necessary for  $n > 2n' + 2$ ,  $n' = 0, 1, 2, \dots$  and consequently glory rays with  $n' > 0$  have 4 or more internal reflections. We have extended the physical-optics approximation described in Sec. II and III to include rays with  $n' > 0$  and find that their contribution to the total glory scattering from fluid spheres is significantly smaller than that of rays with  $n' = 0$ . Consequently, for reasons of brevity and simplified notation, we will only describe the glory scattering due to rays with  $n' = 0$  which is the class of rays illustrated in Fig. 1. Irrespective of the value of  $n'$ , as  $n \rightarrow \infty$ ,  $\theta_n \rightarrow \theta_c$ .

Consider rays which lie close to a glory ray; e.g., the dashed lines near the  $n = 3$  glory ray in Fig. 1. The incident wavefront bounded by these rays is an annular ring which corresponds to wavelet  $de$  in Fig. 1. The corresponding wavefront is toroidal when it leaves the sphere and it corresponds to curved wavelet  $d'e'$ . This wavelet is toroidal because the figure may be rotated around the  $CC'$  axis. The  $n$ th toroidal wavefront appears to originate at a virtual ringlike source at  $F_n$ . Each source forms a virtual focal circle. Rays in the portion of the outgoing wavelet  $F'd'$  cross the backward axis when they are extended.

When the scattering amplitude from a penetrable sphere is computed via ray optics, the amplitude diverges as the observation point approaches the backward axis [see e.g., Ref. 1 (Sec. 12.21), Ref. 9 (Sec. IC3), or Ref. 13

(Sec. VIII)]. This divergence is the manifestation of the axial focusing and it also affects the scattering along the forward axis.<sup>6,9</sup> This divergence is also present in the classical description of scattering from a central potential where the well known differential cross section is<sup>7</sup>

$$\frac{d\sigma}{d\Omega} = \frac{1}{\sin\phi} \sum_i b_i |db_i/d\phi| \quad (6)$$

where the sum is over the different particle trajectories which are scattered by an angle  $\phi$  and  $b_i$  is the impact parameter of the  $i$ th class of trajectory. Axial focusing is predicted for those rays with  $b_i |db_i/d\phi| \neq 0$  as  $\phi \rightarrow \pi$  (backscattering) or  $\phi \rightarrow 0$  (forward scattering).

The cause of the focusing can be seen by rotating Fig. 1 about the CC' axis. Follow adjacent rays having infinitesimally different azimuthal angles but having the same angle of incidence  $\theta$ . When this  $\theta$  is slightly less than the  $\theta_n$  of some "glory ray," the adjacent rays cross the axis at a common point after they leave the sphere. (This can be seen by extending the line  $F_3 d'$ .) This crossing of azimuthally adjacent rays gives rise to the geometrically predicted divergence of the energy density on the axis.

The method for correcting for this divergence was suggested by Van de Hulst.<sup>1,12</sup> It makes use of a physical-optics approximation<sup>4-6</sup> which involves (a) the computation of amplitudes in an exit plane near the sphere via ray optics, and (b) allows these waves to diffract to the observation point. This method will be illustrated for glory rays which give rise to toroidal wavefronts such as those shown in Fig. 1. It will be shown in Sec. V, however, that as  $M \rightarrow M'_n$ , the  $n$ th wavefront is no longer toroidal.

There are rays and types of scatterers for which there is no geometrically predicted focusing. There is no focusing of backscattered axial rays except for certain  $M \geq 2$  (e.g.,  $n = 2$  and  $M = 2$ , see Ref. 14). The  $n = 0$  ray reflects without entering the sphere. To an external observer, its

reflection appears to come from a point-like source at  $A_0$  (see Fig. 1). It is also evident that when a plane wave is incident on a cylinder (with  $M < 1$ ) and propagating in a direction perpendicular to the cylinder's axis, there will be no focusing of the backscattering.<sup>8,9</sup> Figure 1 is applicable but with rotation about the CC' axis no longer allowed. Backscattered rays appear to originate from virtual line sources located, e.g., at  $A_0$  and the  $F_n$ . It is evident from asymptotic formulations of scalar wave scatter by cylinders<sup>15,16</sup> that the geometric scattering from a fluid cylinder does not diverge as  $\gamma \rightarrow 0$ .

## II. Amplitude and Phase in the Exit Plane

In this section we use ray optics to describe the amplitude and phase of the glory waves in the exit plane. It is convenient for this plane to be the one which touches C' with its normal parallel to the propagation direction of the incident wave. Its projection onto Fig. 1 is the dashed vertical line. After the incident ray crosses the dashed vertical line, the propagation phase delay for reaching the exit plane is:

$$\eta = k[a(1 - \cos\theta) + 2anM \cos\gamma + w] \quad (7)$$

where (Fig. 2)  $w$  is the distance traveled by the ray from the exit point on the sphere to the exit plane:

$$w = a(1 - \cos\beta) \sec(\theta - \beta). \quad (8)$$

The ray crosses the exit plane at a radius  $s$  from C' where from Fig. 2

$$s = a[\sin\beta - (1 - \cos\beta) \tan(\theta - \beta)] \quad (9)$$

The radius of the  $n$ th focal circle is  $b_n = a(\sin\theta_n)$ . As is evident from Fig. 1 and by direct computation,  $d\eta/ds = 0$  when  $s = b_n$ . The radius

$\alpha_n$  of the toroidal wavefront at the exit plane is obtained by computing the wavefront's curvature:

$$\alpha_n = k(d^2\eta/ds^2)^{-1}, \quad s = b_n, \quad (10a)$$

$$= a[1 + \frac{1}{2}(n\tau - 1)^{-1} \cos\theta_n], \quad (10b)$$

where  $\tau = \tan v_n / \tan \theta_n$  and  $v_n$  is given by (1) evaluated at  $\theta_n$ , the glory ray condition. The proof of Eq. (10b) is outlined in Appendix A. The spreading of the wavelet  $de$  at the exit plane is characterized by:

$$q_3 = \lim_{(de) \rightarrow 0} \frac{(d'e')}{(de)} = \lim_{(de) \rightarrow 0} \frac{|s(e') - s(d')|}{s(e) - s(d)} \quad (11)$$

where  $(d'e')$  and  $(de)$  are the arc and linear lengths of the outgoing and incoming wavelets, respectively, and  $s$  is the distance from  $C'$  to the indicated points of contact with the dashed plane. From symmetry arguments, the rightmost side of (11), when generalized to arbitrary  $n$ , becomes:

$q_n = |\lim[b_n - s(\theta)]/(b_n - a \sin\theta)|$ , as  $\theta \rightarrow \theta_n$  where  $s$  is an implicit function of the ray's original angle of incidence via (1), (3), and (9).

Application of L'Hospital's rule to this limit (see Appendix A) gives:

$$q_n = |1 + 2(n\tau - 1)\sec\theta_n| = |\alpha_n'(\alpha_n - a)|. \quad (12)$$

With  $M < 1$ ,  $\alpha_n > a$  for all finite  $n$  (and  $n'$ ) so that the absolute value signs in (12) are not needed; for ranges of  $M > 1$ , however, we find some  $[\alpha_n'(\alpha_n - a)]$  are negative.

Let  $p_I \exp(-i\omega t)$  denote the incident pressure in the dashed plane through  $C'$  in Fig. 1 where  $\omega$  and  $p_I$  are the frequency and amplitude of the wave. Ray optics gives the following amplitude in the exit plane for the

nth toroidal wave:

$$p_n'(s) = \frac{p_I B(s)}{q_n^{1/2}} e^{i[\eta_n + \mu_n + k(s - b_n)^2/2a_n]} \quad (13)$$

where the toroid has been approximated by a quadratic surface. This approximation introduces a negligible phase error provided  $k(s - b_n)^4 \ll |\alpha_n^3|$ . The phase factor  $\eta_n$  is the propagation phase delay of the glory ray:

$$\eta_n = 2ka(1 - \cos\theta_n + nM\cos\nu_n) \quad (14)$$

and  $\mu_n$  is the phase shift due to the crossing of focal lines.<sup>1</sup> The  $q_n^{-1/2}$  factor accounts for the change in the area of the wavefront.

The factor  $B(s)$  accounts for the reduction in amplitude due to the partial transmission or reflection of the wave at each interface. We approximate this by repeated use of the internal reflection coefficient for pressure at a plane surface<sup>17-19</sup> as a function of the external angle  $\theta$

$$R(\theta) = \frac{(M^2 - \sin^2\theta)^{1/2} - T\cos\theta}{(M^2 - \sin^2\theta)^{1/2} + T\cos\theta} \quad (15)$$

where  $T = \rho_i/\rho_o$  and  $\rho_i$  and  $\rho_o$  are the densities of the inner and outer fluids, respectively. In (15),  $\theta$  is chosen to be angle of incidence of the ray which crosses the exit plane at  $s$ . Symmetry relations<sup>17,18</sup> between the transmission and reflection coefficients yield the following combined coefficient

$$B(s) = R(\theta)^{n-1} [1 + R(\theta)][1 - R(\theta)] \quad (16)$$

The phase shift  $\mu_n$  accounts for the phase advance of  $\pi/2$  associated with each crossing of a focal curve prior to reaching the exit plane. (This shift occurs due to vanishing of the wavelet's area at each focal curve.<sup>1,19</sup>)

From Fig. 1 it is evident that there are two types of curves. One type, at points  $L_1$  in Fig. 1, is due to the intersection of initially adjacent rays which lie in the same meridional plane. There are  $n - 1$  focal curves of this type when  $M < 1$ . The second type is due to axial focusing of rays within the sphere. There is one focus of this type each time the internal ray intersects the axis; this occurs once when  $n' = 0$ . This is the point  $L_2$  for the  $n = 3$  ray in Fig. 1. The total shift becomes  $\mu_n = -n\pi/2$ . (This result differs from that given in Ref. 1, Sec. 12.22 as Van de Hulst was concerned with the phase shifts at a distant observer.)

Evaluation of the constants  $b_n$ ,  $a_n$ ,  $q_n$ , and  $\eta_n$  requires that (1) through (3) be solved for  $\theta_n$  with  $\gamma = 0$ . With  $n = 3$  or 4 the system of equations reduces to a cubic equation which leads to the following result<sup>5</sup>

$$\sin^2 \theta_n = h_n' M^2 \{1 - h_n' \cos[(\Gamma_n + \pi)/3]\} \quad (17)$$

$$\Gamma_3 = \arccos[(1 - M^2)h_3^{-3}] \quad (18a)$$

$$\Gamma_4 = \arccos[(27/16)M^2 - 1] \quad (18b)$$

where  $0 \leq \Gamma_n \leq \pi$ ,  $h_3' = 1/2$ ,  $h_3 = [1 - 3^{-1}M^2]^{1/4}$ ,  $h_4' = 2/3$ , and  $h_4 = -1/2$ .

When  $n > 4$ , we solve the system iteratively for  $\theta_n$  by choosing  $\theta_{n-1}$  as the first estimate of  $\theta_n$ .

### III. Diffraction and the Far-Field Scattering Amplitude

#### A. Stationary-Phase Approximation for the Backscattered Amplitude

The amplitude  $p_n$  at the observation point  $Q$  can be expressed in terms of a diffraction integral of  $p_n'$  in the exit plane (the  $x'y'$  plane in Fig. 3). In Fig. 3 the  $z$  axis is the extension of the  $CC'$  axis and the

backscattering angle  $\gamma$  is measured with respect to  $C'$  and the  $z$  axis. The  $y'$  axis may be chosen to be the dashed vertical axis in Fig. 1. (Unlike the corresponding optics problem in which polarization breaks the symmetry,<sup>4</sup> here the orientation of the  $y'$  axis is arbitrary.) The Fraunhofer approximation<sup>19,20</sup> for  $r'$  gives  $r' \approx r - [(xx' + yy')/r]$  and it gives the following approximation of the diffraction integral for  $p_n$

$$p_n = 2\pi(i\lambda r)^{-1} e^{ikr} F, r \gg ks_{\max}^2, \quad (19)$$

$$F(x, y) = \frac{1}{2\pi} \iint_{x'^2 + y'^2 \leq s_{\max}^2} p_n'(x', y') e^{-ik(xx' + yy')/r} dx' dy'. \quad (20)$$

where  $s_{\max}$ , the radius of the domain of integration, is sufficiently large that the contribution to the diffracted amplitude from points outside of  $s_{\max}$  is negligible. In addition to making use of the Fraunhofer approximation, (19) neglects any corrections to the amplitude due to the obliquity between  $Q$  and the wavefront in the exit plane. We anticipate the result below that the phase of the integrand is stationary in the region of applicability of the approximations leading to (13). Consequently we extend  $s_{\max}$  in (20) to  $\infty$  and make use of the circular symmetry of  $p_n'$  by writing  $F$  in terms of radial and azimuthal integrals<sup>20,21</sup>

$$F(\gamma) = \int_0^\infty s p_n' W(s, \gamma) ds \quad (21)$$

$$W(s, \gamma) = \frac{1}{2\pi} \int_0^{2\pi} \exp[-ik\Gamma \cos(\psi - \xi)] d\psi = J_0(u) \quad (22)$$

where  $\Gamma = [(x^2 + y^2)/r^2]^{1/2} = \sin\gamma$ ,  $u = ks\Gamma$ , and  $\psi$  is the azimuthal angle of  $(x', y')$ . Due to symmetry,  $F$  and  $W$  do not depend on the azimuthal angle  $\xi$  of  $Q$ .

Since  $W$  is given by the zero-order Bessel function  $J_0(u)$ ,  $F$  is the Hankel transform<sup>20,21</sup> of  $p_n'$ . The phase of  $p_n'$  is stationary when  $s = b_n$  and we use the stationary phase approximation (SPA) of  $F$ . The amplitude of  $p_n'$  is proportional to  $B$  which is a slowly varying function of  $s$  near  $b_n$  except when  $\theta_n$  is close to the critical angle  $\theta_c$ . As  $n \rightarrow \infty$ , recall that  $\theta_n \rightarrow \theta_c$ ,  $R \rightarrow \pm 1$ , and  $B \rightarrow 0$ . Consequently, the strongest  $p_n$  are those with small  $n$  where  $B$  is sufficiently slowly varying that it may be removed from the integrand. These approximations give

$$F \approx p_I B(b_n) q_n^{-1/2} \exp[i(\eta_n + \nu_n)] I \quad (23)$$

$$I = \int_0^\infty s J_0(u) \exp[ik(s - b_n)^2/2a_n] ds \quad (24)$$

where  $q_n^{-1/2}$  has also been removed from the integrand since the spreading of the wavefront has been approximated by (12) which is the value at  $s = b_n$ . The SPA of  $I$  is (see e.g. Ref. 22, Sec. 4.2c):

$$I \approx b_n (kb_n)^{-1/2} \{(2\pi|a_n|b_n)^{1/2} J_0(u_n) e^{i\pi/4} + o(kb_n)^{-1}\} \quad (25)$$

where  $u_n = kb_n$  and the order of the correction term was obtained by noting that the lowest order corrections from the endpoints of (24) vanish. The SPA requires, however, that  $J_0(u)$  be slowly varying near  $u = u_n$  and consequently that  $\gamma$  be small. The condition on (19) may be written  $r \gg kb_n^2$  since  $F$  is dominated by contributions to the integral with  $s \approx b_n$ .

#### B. Determination of the Phase from Properties of the Angular Spectrum

When  $Q$  is not close to the backward axis, (25) does not yield the correct phase for  $p_n$  due to the requirement that  $u_n$  be small. The phase correction is determined here by shifting the plane of integration to that of

the focal circle. (The point at which the axis crosses this plane will be denoted by  $C_n$ ;  $C_3$  is shown in Fig. 1.) Since we let  $s_{\max} \rightarrow \infty$  in (20),  $F$  is a Fourier transform which expresses the planewave angular spectrum of  $p'_n$ . The spectrum in the exit plane is related to the spectrum  $F_n$ , determined in the shifted plane, of the virtual source appropriate for the shifted plane. The relation, which is well known in optics,<sup>21</sup> is given by

$$F = \exp(ik\alpha_n \cos\gamma) F_n \quad (26)$$

where  $\alpha_n$  is the distance between the two planes and  $ik\alpha_n \cos\gamma$  is the phase shift of a planewave, tilted at an angle  $\gamma$  with respect to the axis, as it travels from the plane at  $C_n$  to the one at  $C'$ .

In the shifted plane, the virtual source is a circle whose spatial properties are those of the radial  $\delta$  function:  $\delta(s - b_n)$ . Writing  $F_n$  in the form of a Hankel transform gives:

$$F_n = D_n \int_0^\infty s J_0(u) \delta(s - b_n) ds = D_n b_n J_0(u_n) \quad (27)$$

where  $D_n$  is a complex constant which has been determined by requiring  $D_n b_n J_0(u_n) \exp(ik\alpha_n) = F$  via (23). This procedure, combined with (26) and (19), gives:

$$p_n = p_1 [(a/2r) \exp(ikr)] g_n \quad (28)$$

$$g_n = (ka)^{1/2} E_n B(b_n) J_0(u_n) e^{i[\eta_n + \lambda_n + \phi_n - \frac{1}{4}\pi]} \quad (29)$$

$$\phi_n = -k\alpha_n (1 - \cos\gamma) \quad (30)$$

$$E_n = 2b_n (2\pi|\alpha_n|/q_n)^{1/2} a^{-3/2} \quad (31a)$$

$$= 2(b_n/a) [2\pi|(\alpha_n/a) - 1|]^{1/2} \quad (31b)$$

where (31b) makes use of (12). The phase factor  $\varphi_n$  was not present in (25). An equivalent phase factor may be derived directly from an SPA of (24) by assuming that  $u_n$  is large. This derivation is outlined in Appendix B.

In (29),  $B(b_n)$  is given by (16) with  $\theta = \theta_n$ . The SPA result given above requires  $|R(\theta_n)|$  to be not too small and hence that  $\theta_n$  is not close to Brewster's angle<sup>17</sup>  $\theta_B$  (known also as the angle of intromission). This angle is defined as the solution of  $R(\theta_B) = 0$ ; inspection of (15), gives  $\sin^2 \theta_B = (M^2 - T^2)/(1 - T^2)$ . If  $T \leq M < 1$  or if  $T \geq M > 1$ , then  $\theta_B$  exists.

When  $M < 1$ , all  $a_n$  are positive. If  $a_n < 0$  (which occurs for certain  $M > 1$ ), the signs of the  $\pi/4$  phases in (25) and (29) should be reversed.<sup>22</sup>

### C. The Axial Rays

Since the axial rays are unfocused, their far-field amplitudes and phases can be computed directly from ray optics.<sup>1,13</sup> Figure 4 defines the distances needed to compute the phase difference  $\zeta_0$  between the  $n = 0$  reflected ray and the propagation delay from  $C'$  to  $Q$ . Using our (...) notation for distance gives  $\zeta_0 = k[(234) - (C'1)]$ ; this can be written

$$\zeta_0 = 2ka[1 - \cos(\gamma/2)] - ka(1 - \cos\gamma) \quad (32)$$

by using the geometric results  $\theta = \gamma/2$  and  $(C'1) = (56)$ . The far-field pressure due to each axial ray is  $p_I[(a/2r) \exp(ikr)]f_n$  where the reflected ray has the following form function when  $ka$  is not small:

$$f_0 = -R(\theta = \gamma/2)e^{i\zeta_0}. \quad (33)$$

The minus sign results from our definition that Eq. (15) describes internal reflections. When  $\gamma$  is small, the reflected wave appears to come from  $A_0$  which (as  $\gamma \rightarrow 0$ ) is a distance<sup>23</sup>  $a/2$  from  $C$ .

The form functions  $f_n$  ( $n = 2, 4, \dots$ ) of the other axial rays may be found by computing divergence factors<sup>1</sup> and the phase shifts due to path lengths and foci.<sup>1</sup> It is not generally feasible to express the ray's angle of incidence  $\theta$  as a function of  $\gamma$ ; this necessitates either the numerical solution of transcendental equations or the use of approximations. An approximate description of  $f_2(\gamma)$  is given in Appendix C. A description with  $\gamma = 0$  of electromagnetic axial rays from a dielectric sphere<sup>14</sup> can be modified to give the following acoustic result when  $ka \gg 1$

$$|f_n(\gamma = 0)| = |M(n - M)^{-1} R(0)^{n-1} [1 - R(0)^2]|. \quad (34)$$

For the examples to be described in this paper  $f_0$  and  $f_2$  are similar in magnitude; for  $n \geq 4$ ,  $|f_n| \ll |f_0|$  so that approximations for those  $f_n(\gamma)$  will not be given here.

#### D. The Combined Scattering Amplitude

The above results may be combined to give the following approximation for the pressure amplitude in the far field

$$p(r, \gamma) = p_1 [(a/2r) \exp(ikr)] f, \quad r \gg ka^2 \quad (35)$$

$$f(\gamma) \approx f_0 + f_2 + \sum_{n=3}^N g_n, \quad M < 1 \quad (36)$$

where  $N$  should be sufficiently large to approximate an infinite series.

The normalization for the form function  $f$  has been chosen such that  $f_0 = 1$  for geometric reflection from a fixed-rigid sphere of the same size. The salient feature of (29) is that  $|g_n(\gamma = 0)| \propto (ka)^{1/2}$  while the  $|f_n|$  do not depend on  $ka$ . Consequently the backscattering from large fluid spheres will be dominated by contributions of the diffracted glory waves provided the

attenuation of sound is negligible. As  $ka \rightarrow \infty$ , the glory contributions to (36) diverge; this divergence, a consequence of axial focusing, was also evident in the purely geometric scattering; e.g., Eq. (6).

When  $ka$  is not large, (36) must be modified to include terms due to circumferential waves. Our tests of (36) had  $ka \geq 100$  and, as a consequence of the largeness of  $ka$ , circumferential waves<sup>15,19</sup> and associated resonances<sup>24</sup> should experience significant radiation damping. The backscattering from spheres due to circumferential waves will, nevertheless, be assisted by diffraction-limited axial focusing as is the case for electromagnetic scattering.<sup>1,3,12</sup> Circumferential wave contributions to the scattering from elastic objects are significant for  $ka$  as large as<sup>25,26</sup> 200; however, their significance to the scattering from large fluid objects with  $\rho_i \approx \rho_o$  is not well explored.

The conventional description of the scattering<sup>10,13,24</sup> references the phase of the incident wave to the sphere's center C. It also uses distances and angles with respect to C so that  $r$  becomes  $(CQ)$  and  $\gamma$  becomes the polar angle of Q with C as the origin. For the far-field scattering the form of (35) is retained with  $f$  replaced by  $f_C(\gamma) = f(\gamma) \exp[i\zeta_C]$  where

$$\zeta_C = -ka(1 + \cos\gamma) \quad (37)$$

is the negative of the phase shift for the distance  $(C'C_5)$  in Fig. 4. The  $\gamma$ -dependent phase shift for the reflected ray becomes  $\zeta_0 + \zeta_C = -2ka \cos(\gamma/2)$  which agrees with the conventional<sup>13</sup> result; for the glory terms it becomes  $\zeta_n + \zeta_C = -k[2a + (a_n - a)(1 - \cos\gamma)]$ . (When  $a_n = a$ , the latter result follows from elementary considerations.) Since the modulus of the form function is not altered by the transformation from  $C'$  to C, it is possible to compare  $|f|$  from (36) directly with  $|f_e|$  where  $f_e$  is the exact result of the partial-wave theory.<sup>10,18,24</sup>

IV. Discussion of Model and Comparison with Exact Scattering from Spheres with  $M < 1$

In this section we compare Eq. (36) with the modulus of the exact form function  $f_e$ . The partial-wave series for  $f_e$  was summed by using the computer algorithm described in the appendix of Ref. 18. The number of partial-waves included exceeded  $ka + 4.05 (ka)^{1/3}$  to ensure adequate convergence.<sup>18</sup> This algorithm was limited to the case of equal inner and outer fluid densities ( $\rho_i = \rho_o$ ) and the  $|f_e|$  presented here and in Sec. V are limited to this case.

Tables I and II are representative of model results for form function moduli of axial and glory terms and for the focal circle parameters. These tables should be examined in conjunction with Fig. 5-7. In each of the figures, the largest  $N$  was chosen to be a power of 2 such that an additional doubling of the largest  $n$  in (36) resulted in a new curve (not shown) which differed imperceptibly from the dotted curve.

The value of  $M$  in Fig. 5 was selected such that the modulus of  $f_4$ , the strongest of the omitted axial ray amplitudes, is especially small in comparison with  $|g_3(\gamma = 0)|$ . The main result of Fig. 5a is that (36), with  $N \geq 16$ , gives an amplitude which is nearly identical to the exact result for the range of  $\gamma$  plotted. This confirms, with very large  $ka$ , our model result for the amplitude and relative phases of the  $f_n$  and  $g_n$ . Note also that  $|f|$  for  $\gamma \geq 0.2^\circ$  is dominated by the interference of  $g_3$ ,  $f_0$ , and  $f_2$ ; for  $\gamma < 0.2^\circ$ , however, glory terms with  $n > 3$  are significant. Figure 5b confirms that the principal features of  $|f_e|$  are described by the model. Note that the dip in  $|f_e|$  near  $12.5^\circ$  is largely due to the destructive interference of axial rays. Though we have previously modeled individual contributions,<sup>4-6,8</sup> Fig. 5 is the first direct confirmation that a sum of axial and glory waves can account for most of the backscattering from spheres with  $M < 1$ .

Figures 6 and 7 confirm again that the principal features of  $|f_e|$  are described by the model. In Fig. 6a and 7, discrepancies between the modeled and exact scattering are evident, especially at  $\gamma = 0$ . The causes of these discrepancies are not known. Equation (36) has also been tested by including a sum of glory terms with  $n' = 1$  (which have  $n \geq 5$ ) but the resulting shift in  $|f|$  is much too small to account for the discrepancies. Though the individual  $|f_n|$  with  $n \geq 4$  are small, it is plausible that the coherent sum of omitted axial terms could account for significant part of the discrepancy. It is apparent that the omission of circumferential waves from the model is acceptable in Fig. 5 and 6b; this omission could account for some of the discrepancies evident in Fig. 7.

Some noteworthy features of the modeled scattering are: (i) the width of the backward peak of the scattering is roughly  $\propto 1/(ka)$  but the details of the structure are highly dependent on  $ka$  according the interference of the terms in (36); (ii) there is a tendency for the width of the peak to increase with decreasing  $b_3$  and hence, decreasing  $M$ ; (iii) though the  $|g_n(\gamma = 0)| \propto (ka)^{1/2}$ ,  $|f|$  is not  $\propto (ka)^{1/2}$  due to the  $ka$  dependence of the interference between the  $g_n$  and the  $ka$ -independent  $f_n$ ; (iv) form function moduli can exceed (e.g. Fig. 6a) or be close to (e.g. Fig. 6b, 7b) unity which is the geometric result for reflection from a fixed-rigid sphere of the same size. This enhancement is a manifestation of diffraction-limited axial focusing of the back-scattering. It is possible, however, for the various glory terms to interfere so as to produce a minimum in  $|f|$  for  $\gamma = 0$ ; this is evident in plots of  $|f|$  and  $|f_e|$  for  $M = 0.5$  with  $ka = 1000$  which are not shown here.

Some aspects of the convergence of the series in (36) could be noted. As  $n \rightarrow \infty$ ,  $b_n \rightarrow M$  and  $\eta_n \rightarrow \eta_\infty$  where

$$\eta_\infty = 2ka[(1 - \cos\theta_c) + M(\pi - \theta_c)] . \quad (38)$$

This is the propagation phase shift a ray would have if it entered and exited from the sphere at the critical angle  $\theta_c$  and it traveled a circumferential path with a phase velocity of  $c_1$ . Numerical tests suggest that it is sufficient to terminate the series when<sup>27</sup>  $(\eta_\infty - \eta_n) \leq 1$  radian. The omitted terms tend to cancel because of the alternating sign of  $B(b_n)$  and the periodicity of the phase factor  $\exp(i\mu_n)$  associated with the crossing of internal foci. As  $n$  increases,  $|g_n|$  decreases due to decreasing  $|B(b_n)|$  and increasing  $q_n$ ; see Tables I and II. When  $\rho_1 \neq \rho_0$ , the  $B(b_n)$  are changed but the geometric parameters are not.

It may be possible to arrive at (29) for  $g_n$  from the asymptotic evaluation (at large  $ka$ ) of the exact partial-wave sum. Glory ray amplitudes should be describable by saddle-point contribution to a contour integral from the Watson transformation<sup>3</sup> of the exact sum. Our use of the physical-optics approximation in Sec. II and III, though less direct, manifests the physical significance of the parameters  $a_n$ ,  $b_n$ ,  $q_n$ ,  $\phi_n$ , and  $\mu_n$ . Furthermore, our approach bypasses the difficulties with the asymptotic method noted in Ref. 13 and it may be extended to the near field by replacing (19) by a Fresnel transform.<sup>19-21</sup> It may be important that  $\rho_1$  and  $\rho_0$  be similar in magnitude for otherwise resonances<sup>24</sup> (as in a gas bubble) may be significant. The lower limit on  $ka$  for which (36) is applicable is not known; the physical-optics method was found to be useful,<sup>18</sup> depending on  $M$ , for the description of near critical-angle scattering when  $ka \geq 25$ .

The physical-optics model may be used to approximate the scattering of tone bursts where  $k$  is obtained from the average frequency of the incoming burst. The time delays of discrete echoes follows from the propagation phase shifts  $\eta_n$ ,  $\phi_n$ , and  $\zeta_n$ . Shapes of discrete glory echoes will differ from

the incoming bursts<sup>11</sup> due to the  $k$ -independent phase shifts, the  $\mu_n$  and  $\pi/4$  terms in (29); the scattered burst is related to the incoming signal through superposition of time-shifted incoming and Hilbert-transformed signals.<sup>19</sup>

An extensive test of (36) could be carried out by repeating the comparisons in Figs. 5-7 with several smaller  $ka$ . This would be inefficient to do at present since the  $|f_e|$  and  $|f|$  curves are plotted using separate computer systems. Figures 5-7 were made by overlaying and tracing the curves.

#### V. Spheres with $M > 1$ and Combined Rainbow and Glory Scattering

In this section we summarize the results of exact calculations of backscattering from large fluid spheres with certain  $M > 1$  and we model the enhancement of backscattering due to rainbow rays. As described in Sec. I, the class of glory rays with  $n' = 0$  and  $n \geq 3$  are not limited to  $M \leq 1$ ; they also exist for  $1 < M \leq M'_n$  where the upper bounds are given by (4) and (5) for  $n = 3$  and 4. Form functions for this class of rays are given by (29) except when the ray has  $n$  internal chords and  $M \approx M'_n$ . There is an additional caveat to be noted:<sup>5</sup> when  $M'_n < M < M'_n'$  there is second class of rays having  $n$  internal chords which also cross the axis once. Here  $M''_n = \csc[(n-1)\pi/2n]$  is the value of  $M$  for which (1) and (3) give  $\theta = \beta = \pi/2$ . When  $n = 3$ , the angle of incidence of this second backscattered ray is given by (17) with  $(\Gamma_3 + \pi)/3$  replaced by  $\pi + (\Gamma_3/3)$ .

The following comparison of ray properties for the two classes (each with  $n$  chords), will facilitate a description of the unusual backscattering properties of spheres having  $M = M'_n$ . Let  $\tilde{b}_n = \sin\theta_n$  and  $\tilde{a}_n$  [from Eq. (10)] denote the focal parameters for the new class of ray while  $b_n$  and  $a_n$  denote those for the original type. With  $M''_n < M < M'_n$ , the parameters obey the

following inequalities:  $b_n < \tilde{b}_n < a$ ,  $\alpha_n > a$ , and (for  $M$  not too close to  $M'_n$ )  $\tilde{\alpha}_n > 0$ . As  $M \rightarrow M'_n$ , Eqs. (1), (3), (10), and (17) lead to the results:  $\tilde{b}_n \rightarrow b_n$ ,  $n\tau \rightarrow 1$ ,  $\alpha_n \rightarrow \infty$ ,  $\tilde{\alpha}_n \rightarrow \infty$  and  $q_n \rightarrow 1$ . The divergence of the distances to the focal circles gives rise to the erroneous prediction by (31) that  $E_n$ , and hence  $g_n$  also diverge for each of these rays. The present physical-optics approximation fails because the glory wave is no longer toroidal as required by (13). Numerical computations applied to the  $n = 3$  ray and the case  $M = M'_3$  give the following limit as  $s \rightarrow b_3$ :  $[n(s) - n_3]/(s - b_3)^3 \rightarrow \Lambda_3 k a^{-2}$  where the dimensionless constant  $\Lambda_3 \approx -26.6$ . Hence the wavefront is cubic which is characteristic of a "rainbow" or "stationary" ray. Figure 8 shows this ray.

It is well known that scattering is enhanced<sup>1,7,13,23</sup> in the vicinity of a rainbow ray. Rainbow rays have  $dy/d\theta = 1 - (d\beta/d\theta) = 0$ . This is equivalent to the condition  $|db_1/d\phi| \rightarrow \infty$  in (6). These conditions require that<sup>5,13</sup>  $\sin^2 \theta = (n^2 - M^2)/(p^2 - 1)$ . We have verified<sup>5</sup> that the glory rays with  $M = M'_n$  and  $n = 3$  and 4 satisfy this requirement; geometrical considerations suggest that it is also met when  $n > 4$ . Consequently when  $M \approx M'_n$ , the back-scattering is doubly enhanced relative to that due to axial rays: once due to axial focusing and once due to the rainbow caustic.

We have developed a physical-optics approximation for  $g_n$  for the special case  $M = M'_n$ . The principal change of the approximation described in Sec. IIIA is to replace (24) by

$$I = \int_0^\infty s J_0(u) e^{i\Lambda_n k(s-b_n)^3/a^2} ds \approx b_n J_0(u_n) I_n \quad (39)$$

where the SPA has been used to remove from the integral, that part of the integrand which is assumed to be slowly varying near  $s = b_n$ . The remaining integral is

$$I_R = \int_0^\infty e^{i\Lambda_n k(s-b_n)^3/a^2} ds. \quad (40)$$

In the analysis which follows, we assume that  $\Lambda_n < 0$ , which is the case for  $n = 3$ . It can be shown that the general form of the final result, Eq. (42), does not depend on the sign of  $\Lambda_n$ . Changing the integration variable to  $s = (s - b_n) (-3\Lambda_n a^{-2})^{1/3}$  reduces  $I_R$  to an incomplete Airy integral in which the lower limit of integration is  $s_n = -b_n (-3\Lambda_n a^{-2})^{1/3}$ . As  $k^{1/3} s_n \rightarrow -\infty$ , the incomplete integral has an asymptotic approximation [Eq. (10) of Ref. 28] in terms of the complete Airy function  $Ai$  which gives

$$I_R \approx \frac{a}{\Lambda_n^{1/3}} \left[ 2\pi Ai(0) + i \left( \frac{a}{b_n} \right)^2 \frac{e^{-i(\Lambda_n'/3)(b_n/a)^3}}{\Lambda_n^{2/3}} \right] \quad (41)$$

where  $Ai(0) \approx 0.35503$  and  $\Lambda' = -3ka\Lambda_n$ . These approximations give the following normalized form function in place of  $g_n$  when  $M = M'_n$

$$g_{rn} \approx -i(ka)^{2/3} E_{rn} B(b_n) J_0(u_n) e^{i[n_n + \mu_n]} \quad (42)$$

$$E_{rn} = 4\pi Ai(0) b_n / [a(-3\Lambda_n)^{1/3}] \quad (43)$$

where we have used the geometric result that  $q_n \rightarrow 1$  and the second term in (41) has been omitted because of its small magnitude in cases to be considered here. It is to be expected that  $g_{rn} \propto (ka)^{2/3}$  because the enhancement of the diffracted amplitude of a nonbackscattered rainbow<sup>1,3,23</sup> is  $\propto (ka)^{1/6}$ .

The results of this model when  $n = 3$  are compared with  $|f_e|$  in Fig. 9. Away from  $\gamma = 0$ , a complete approximation for  $g_{rn}$  may contain a  $\gamma$ -dependent phase shift similar to the  $\phi_n$  factor in  $g_n$ . Since this shift has not been determined, our comparison is limited to comparing  $|g_{r3}|$  with  $|f_e|$  in cases where  $|f_e| \gg |f_2|$  (which is now the leading axial ray amplitude,

see Table III). Figure 9 demonstrates that (42) describes the main features of the scattering when  $ka = 1000$  but that (42) is relatively incomplete when  $ka = 100$ . This conclusion is also supported from our computations of  $|f_e(\gamma = 0)|$  for several  $ka$  within  $\pm 10$  of 1000 and 100. In each case  $|f_e|$  varied aperiodically with  $ka$ . Near  $ka = 1000$  the extrema were typically between 17.4 and 20.2; near  $ka = 100$ , they were typically between 3.8 and 6.8. These are to be compared with  $|g_{L3}|$  of 18.9 and 4.1 for  $ka$  of 1000 and 100, respectively. That there should be significant corrections to the physical-optics approximation when  $ka = 100$  is to be expected from proximity of  $\nu_3 \approx 55.7^\circ$  to the internal critical angle  $\nu_c = \arcsin(M_3'^{-1}) \approx 57.9^\circ$ . The use of plane-surface reflection coefficients to compute  $B(b_3)$  fails as  $\nu \rightarrow \nu_c$  because tunneling, surface waves, and resonances make curvature an important consideration.<sup>1,3</sup>

Table III includes exact results with other values of  $M$ . For each case  $|f_e|$  was computed for a range of  $\gamma$  sufficient to include several of the backward diffraction maxima; its peak occurred at  $\gamma = 0$  in each case. The relative magnitudes are consistent with the considerations given at the beginning of this section. The rainbow condition is not met when  $M = 1.1$  and the backscattering is weaker than for  $M_3'$ . The backscattering is doubly enhanced when  $M = M_4'$ . It is small when  $M = 1.25$  with  $ka = 1000$  because there is no glory ray having only a few chords (irrespective of  $n'$ ) and circumferential waves experience significant radiation damping.

The combined rainbow-glory enhancement of backscattering is not limited to the precise condition  $M = M_n'$ . Due to diffraction,<sup>3</sup> a rainbow will influence the backscattering when  $d\gamma/d\theta = 0$  in the vicinity of  $\gamma = 0$ . Consequently, backscattering will be enhanced for  $M$  in some range near  $M_n'$  which narrows for increasing  $ka$ . There are other cases of glory enhanced backscattering

outside of the range  $0 < M \leq M'_3$  considered in this paper. The most useful of these may be that due to the  $n = 2$  glory ray for  $\sqrt{2} < M < 2$ .

Our Mie theoretic computations<sup>29</sup> of the backscattering of light from dielectric spheres also demonstrate a combined rainbow-glory enhancement for optical refractive indices of  $M'_3$  and  $M'_4$ .

## VI. Applications to Underwater Acoustics

The models developed in Sec. III and V for glory and rainbow-enhanced glory backscattering are more general than the case of a purely fluid sphere provided focal-circle parameters, attenuation, and coefficients of reflection and transmission are properly modeled. For example, Eq. (29) removes the  $\gamma \rightarrow 0$  divergence of amplitudes backscattered from solid spheres present in the geometric model of Ref. 9; subtleties of this application will be described elsewhere.<sup>11</sup> Spheres have been used as calibration targets for sonar systems<sup>30-32</sup> because of their symmetry; their response is asserted to be more uniform (in regard to variations in the direction of the incoming wave) than the triplane reflector.<sup>31,32</sup> In this section we comment on the design of practical spheres which could be made to exhibit glory enhanced backscattering.

Liquid spheres with  $ka \gtrsim 100$  are too large for surface tension to ensure sphericity. For example, with  $c_0 = 1.53$  m/s (sea water) and  $\omega/2\pi = 100$  kHz, the radius  $\approx 24$  cm when  $ka = 100$ . The target liquid may be contained in a thin elastic shell.<sup>31,32</sup> For ease of transport, the shell's interior may be left unfilled until submersion.<sup>31</sup> In the discussion which follows, shear and longitudinal sound velocities of the bulk shell material will be denoted by  $c_s$  and  $c_\ell$  and the shell's thickness will be denoted by  $h$ ;  $\rho_1$ ,  $a$ , and  $c_1$  are the density, radius, and sound velocities of the inner liquid and  $M = c_0/c_1$ .

For a large sphere, glory rays illustrated in Fig. 1 and 8 exist in the  $h \ll a$  limit. The main difficulty in using Eq. (29) and (42) to estimate the scattering is in the evaluation of  $B(b_n)$  for the transmission through and reflection from the shell. Proper choice of  $h$  could simplify the analysis by facilitating the use of the thin-plate approximation for the transmission and reflection coefficients of flat plates.<sup>17,19</sup> For larger  $h$ , the analysis is complicated since both  $c_g$  and  $c_s$  typically exceed  $c_o$  and  $c_i$ . Furthermore, Lamb modes<sup>24</sup> are launched in the shell at certain angles of incidence.<sup>26</sup> A plausible choice to facilitate transmission into the sphere's interior is to select  $c_s$  somewhat smaller than  $c_o$  and  $c_i$ . (For example, Lexan is a strong material having  $c_s \approx 910$  m/s.) In the case of rainbow-enhanced glory, Fig. 8, the calculation of  $B(b_3)$  may be especially complicated due to the largeness of  $\theta_3$  and  $v_3$ .

A computational demonstration of glory-ray enhanced backscattering may be best achieved by computing the exact scattering from thin, liquid-filled spherical shells by extending the computations in Ref. 33 to  $ka \gtrsim 100$  and certain  $M \neq 1$ . The calculations should include a range of  $\gamma$ . The exact calculation would be most interesting in the case  $M = M_3'$  due to the  $(ka)^{2/3}$  enhancement factor in (42). The possibility of enhanced backscattering from liquid-filled shells with this  $M$  has been previously overlooked. (For example, if it is present, the interpolated target strength versus  $M$  curve in Fig. 5 of Ref. 31 contains serious errors.) Circumferential waves, which are known to influence backscattering from large cylindrical shells,<sup>26</sup> will give rise to axially focused backscattering from spherical shells. The relative importance of ray-optical and circumferential returns may be evaluated by displaying the scattering of a short tone burst as in Ref. 33. Certain inhomogeneous spheres exhibit glory rays and should have enhanced backscattering.<sup>34</sup>

### Acknowledgments

We are grateful to K. L. Williams and S. P. Love for computational assistance and to an anonymous referee of our earlier paper (Ref. 4) for comments concerning the calculation of  $a_n$ . This work was supported by the Office of Naval Research. P. L. Marston is an Alfred P. Sloan Research Fellow.

### Appendix A: Curvature and Spreading of Glory Wavefronts

The wavefront is described by a curve of constant propagation phase delay  $\eta$ . Its curvature at the exit plane is  $1/a = k^{-1} (d^2\eta/ds^2) / [1 + (k^{-1} d\eta/ds)^2]^{3/2}$  where  $s$  is the distance from  $C'$ ;  $\eta$  and  $s$  are given by (7) through (9) as functions of  $\theta$ ,  $\beta$ , and  $v$ , but could, in principle, be written as functions of  $\theta$  only, by making use of (1) and (3). We then have

$$\frac{1}{a} = \frac{(ds/d\theta)(d^2\eta/d\theta^2) - (d\eta/d\theta)(d^2s/d\theta^2)}{k[(ds/d\theta)^2 + (k^{-1} d\eta/d\theta)^2]^{3/2}} \quad (A1)$$

where the differential operator is

$$\frac{d}{d\theta} = \frac{\partial}{\partial\theta} + \left(\frac{dv}{d\theta}\right) \frac{\partial}{\partial v} + \left(\frac{\partial\beta}{\partial v} \frac{dv}{d\theta} + \frac{\partial\beta}{\partial\theta}\right) \frac{\partial}{\partial\beta} \quad (A2)$$

$$= \partial/\partial\theta + \tau \partial/\partial v + (2\pi\tau - 1) \partial/\partial\beta \quad (A3)$$

where (A3) uses (1) and (3) and the definition  $\tau = dv/d\theta = \tan v / \tan \theta$ . The first derivatives in (A1) are

$$(ka)^{-1} \frac{d\eta}{d\theta} = 2(1-\pi\tau)(1-\cos\beta)\sec(\theta-\beta)\tan(\theta-\beta) + (1-2\pi\tau)(\sin\theta-\sin\beta\sec(\theta-\beta)) , \quad (A4)$$

$$a^{-1} \frac{ds}{d\theta} = 2(\pi\tau-1)(1-\cos\beta)\sec^2(\theta-\beta) + (2\pi\tau-1)(\cos\beta-\sin\beta\tan(\theta-\beta)) . \quad (A5)$$

The second derivatives are somewhat longer, but straightforward to calculate.

The interesting cases are the glory rays, occurring when  $\beta = \theta$ ; this condition will be denoted by a subscript  $n$  for the glory ray with  $n$  chords. Since  $(d\eta/d\theta)_n = 0$ , (A1) becomes  $k/a_n = [(d^2\eta/d\theta^2)/(ds/d\theta)^2]_n$ . The derivatives at the glory condition are  $(ds/d\theta)_n = a[2(n\tau-1) + \cos\theta_n]$  and  $(d^2\eta/d\theta^2)_n = 2k(n\tau-1)(ds/d\theta)_n$ . Hence the radius of curvature of the wavefront is given by (10b).

From (9) and (11), the spread of the wavefront may be written as

$$q_n = \lim_{\theta, \beta \rightarrow \theta_n} \frac{\sin\theta_n - [\sin\beta - (1 - \cos\beta)\tan(\theta - \beta)]}{\sin\theta_n - \sin\theta}, \quad (A6)$$

$$= \lim_{\theta, \beta \rightarrow \theta_n} \frac{(d/d\theta)[\sin\theta_n - \sin\beta + (1 - \cos\beta)\tan(\theta - \beta)]}{(d/d\theta)[\sin\theta_n - \sin\theta]} \quad (A7)$$

where (A7) follows from L'Hospital's rule. Application of (A3) gives an expression which reduces to (12).

We have verified (10b), for several values of  $M \neq M'_n$ , with direct numerical computations demonstrating that as  $s \rightarrow b_n$ ,  $[\eta(s) - \eta_n]/(s - b_n)^2 \rightarrow k(2a_n)^{-1}$ . Furthermore, determinations of focal circle locations by direct ray tracing (from large versions of Fig. 1) are in agreement with (10b). Our result for  $q_n$  has also been verified by numerical evaluation of the limit in (11). These tests were merited because quantities equivalent to  $a_n$  and  $q_n$  are given by incorrect expressions in Appendix II of Ref. 23. Those expressions were erroneous due to incorrect formulation of total derivatives; they happen to give the correct ratio  $|a_n|/q_n$ .

#### Appendix B: Angle-Dependent Phase Shift Via the Method of Stationary Phase

The purpose of this appendix is to demonstrate that a modified SPA of (24) yields a phase shift equivalent to (30) and to give insight into the cause

of that shift. The derivation which follows is limited to cases where  $u_n \gg 1$ . In (24), express  $J_0(u)$  using Hankel functions of the first and second kinds.<sup>22</sup>  $J_0(u) = \frac{1}{2}[H_0^{(1)}(u) + H_0^{(2)}(u)]$  and define  $Z_j(u) = H_0^{(j)}(u)\exp(\pm iu)$  with  $j = 1$  and  $2$  (here and below) for the upper and lower sign, respectively. Then (24) is a sum of integrals of the form

$$I_j = \frac{1}{2} \int_0^\infty s Z_j \exp[ik\frac{1}{2}(s-b_n)^2 \alpha_n^{-1} \pm iu] ds \quad (B1)$$

where the stationary phase points of the complex exponentials are at  $s = s_j$  with  $s_j = b_n \mp \alpha_n \Gamma$ . From the asymptotic forms<sup>22</sup> of the  $H_0^{(j)}(u)$  as  $u \rightarrow \infty$ , it is evident that  $sZ_j$  is a slowly varying function of  $s$  near  $s = s_j$  provided  $u_n \gg 1$  and  $|\alpha_n| \Gamma \ll b_n$ . Consequently, in the SPA of (B1), it is appropriate to treat the complex exponential, which differs from that of (24), as the function which oscillates rapidly when  $s \neq s_j$ . Approximating  $I_1$  and  $I_2$  by this procedure gives the following sum:

$$I \approx b_n (2\pi|\alpha_n|/k)^{1/2} J_0(u_n) e^{i(\Phi_n' + \pi/4)} \quad (B2)$$

where terms of order  $\alpha_n \Gamma / b_n$  relative to unity have been neglected and  $\Phi_n' = -\frac{1}{2}k\alpha_n \Gamma^2$ . Replacing (25) by (B2) leads directly to (29) with  $\Phi_n$  replaced by  $\Phi_n'$ . By inspection, when  $\Gamma \ll 1$ ,  $\Phi_n$  and  $\Phi_n'$  are identical up to terms  $\alpha \Gamma^4$ . They give nearly identical results for the conditions under which (29) was tested in Sec. IV. The derivation of  $\Phi_n'$ , however, assumes that both  $u_n \gg 1$  and  $|\alpha_n| \Gamma \ll b_n$  and hence that  $(kb_n)^{-1} \ll \Gamma \ll b_n/|\alpha_n|$ .

The shift of the stationary phase points by  $\pm \alpha_n \Gamma$  has the following physical interpretation. Consider the locations of the effective areas (or Fresnel zones<sup>1</sup>) of the toroidal wavefront which contribute to the scattering to  $Q$ . When  $\Gamma \neq 0$ , these zones are centered on points with  $\psi = \xi$  and  $\psi = \pi + \xi$  where  $\xi$  (Fig. 3) is the azimuth of  $Q$ . The centers of these zones are shifted

away from  $b_n$  by  $\pm \alpha_n \Gamma$ . This shift of the effective areas of the toroidal wave leads to the phase shift  $\varphi'_n$ .

#### Appendix C: Amplitude of the One-Bounce Axial Ray

The purpose of this appendix is to describe an approximation for  $f_2(\gamma)$ . The geometry of the associated ray is shown in Fig. C-1. Let  $\zeta_2$  denote the phase difference between the  $n = 2$  ray and the propagation delay from  $C'$  to  $Q$ . Inspection of Fig. C-1 gives  $\zeta_2 = k[(12) + M(234) + (45) - (C'6)] = 2ka[(1 - \cos\theta) + 2M \cos\gamma] - ka(1 - \cos\gamma)$ . We express  $\zeta_2$  as a function of  $\gamma$  by using an approximation for  $\theta$ . As  $\gamma \rightarrow 0$ , Eq. (1) becomes  $\theta = Mv$  provided  $|M - 1|$  is not large. Eliminating  $v$  from the exact expression  $\gamma = 2(2v - \theta)$  gives

$$\theta \approx M\gamma/(4 - 2M) \quad (C1)$$

From this estimate of  $\theta$ , the complete Eq. (1) is used to obtain  $v$  and  $\zeta_2$  is found via the expression given above. This approximation for  $\zeta_2$  was compared with the exact result (which may be computed as a function of  $\theta$ ). The error is negligible for the range of  $ka$ ,  $\gamma$ , and  $M$  of the computations in Sec. IV. The approximation for  $f_2$  is

$$f_2 \approx R(\theta)[1 - R(\theta)^2][M/(2 - M)]e^{i(\zeta_2 - \pi)} \quad (C2)$$

where the  $-\pi$  phase term results from the crossing of two foci. The factor  $M/(2 - M)$  is the divergence factor<sup>1,13,14</sup> appropriate for  $\gamma = 0$ . Tests indicate that our approximation of this factor by a constant introduces a negligible error in Fig. 5-7. The reflection coefficient was computed via (15) and (C1).

## References

1. H. C. Van de Hulst, Light Scattering by Small Particles (Wiley, New York, 1957).
2. H. C. Bryant and N. Jarmie, "The glory," *Sci. Am.* 231, 60 (July 1974).
3. H. M. Nussenzveig, "Complex angular momentum theory of the rainbow and the glory," *J. Opt. Soc. Am.* 69, 1068-1079 (1979).
4. D. S. Langley and P. L. Marston, "Glory in optical backscattering from air bubbles," *Phys. Rev. Lett.* 47, 913-916 (1981).
5. P. L. Marston and D. S. Langley, "Glory in backscattering: Mie and model predictions for bubbles and conditions on refractive index in drops," *J. Opt. Soc. Am.* 72, 456-459 (1982); In the final section, the equation  $p_T = -1$  should be  $p_T = 1$ .
6. P. L. Marston, D. S. Langley, and D. L. Kingsbury, "Light scattering by bubbles in liquids: Mie theory, physical-optics approximations, and experiments," *Appl. Sci. Res.* 38, 373-383 (1982); P. L. Marston, "Light scattering by bubbles in liquids: comments and application of results to circularly polarized incident light," *Appl. Sci. Res.* (at press).
7. K. W. Ford and J. A. Wheeler, "Semiclassical description of scattering," *Ann. Phys. (N.Y.)* 7, 259-286 (1959).
8. P. L. Marston and L. Flax, "Glory contribution to the backscatter from large elastic spheres," *J. Acoust. Soc. Am. Suppl.* 68, S81 (1980).
9. G. J. Quentin, M. deBilly, and A. Hayman, "Comparison of backscattering of short pulses by solid spheres and cylinders at large  $ka$ ," *J. Acoust. Soc. Am.* 70, 870-878 (1981).
10. V. C. Anderson, "Sound Scattering from a Fluid Sphere," *J. Acoust. Soc. Am.* 22, 426-431 (1950).

11. P. L. Marston, K. L. Williams, and T. J. B. Hanson, "Observation of the acoustic glory: High-frequency backscattering from an elastic sphere," *J. Acoust. Soc. Am.* (to be submitted, also to be presented at the 104th meeting of the *Acoust. Soc. Am.*, Nov. 1982).
12. H. C. Van de Hulst, "A theory of the anti-corona," *J. Opt. Soc. Am.* 37, 16-22 (1947).
13. S. I. Rubinow, "Scattering from a penetrable sphere at short wavelengths," *Ann. Phys. (N.Y.)* 14, 305-332 (1961).
14. J. J. Stephens, P. S. Ray, and T. W. Kitterman, "Far-field impulse response verification of selected high-frequency optics backscattering analogs," *Appl. Opt.* 14, 2169-2176 (1975).
15. D. Ludwig, "Diffraction by a circular cavity," *J. Math. Phys.* 11, 1617-1630 (1970).
16. D. Brill and H. Überall, "Transmitted Waves in the Diffraction of Sound from Liquid Cylinders," *J. Acoust. Soc. Am.* 47, 1467-1469 (1970).
17. L. M. Brekhovskikh, Waves in Layered Media, 2nd ed. (Academic, New York, 1980).
18. P. L. Marston and D. L. Kingsbury, "Acoustic scattering from fluid spheres: Diffraction and interference near the critical scattering angle," *J. Acoust. Soc. Am.* 70, 1488-1495 (1981).
19. A. D. Pierce, Acoustics. An Introduction to its Physical Principles and Applications (McGraw Hill, New York, 1981).
20. A. Papoulis, Systems and Transforms with Applications in Optics (McGraw Hill, New York, 1968).
21. W. T. Cathey, Optical Information Processing and Holography (Wiley, New York, 1974); J. A. Ratcliffe, "Some applications of diffraction theory and their application to the ionosphere," *Rep. Prog. Phys.* 19, 188-267 (1956).

22. L. B. Felsen and N. Marcuvitz, Radiation and Scattering of Waves (Prentice-Hall, New York, 1973).
23. R. G. Kouyoumjian, L. Peters, Jr., and D. T. Thomas, "A modified geometrical optics method for scattering by dielectric bodies," IEEE Trans. Antennas Propag. AP-11, 690-703 (1963).
24. L. Flax, G. C. Gaunaurd, and H. Überall, "Theory of Resonance Scattering," in Physical Acoustics edited by W. P. Mason and R. N. Thurston (Academic, New York, 1981), Vol. 15, pp. 191-294.
25. J. W. Dickey and H. Überall, "Acoustic high-frequency scattering by elastic cylinders," J. Acoust. Soc. Am. 66, 275-283 (1979).
26. L. R. Dragonette, "Evaluation of the relative importance of circumferential or creeping waves in the acoustic scattering from rigid and elastic solid cylinders and from cylindrical shells," NRL Report 8216 (Naval Research Laboratory, Washington, D.C., 1978).
27. This condition appears to ensure that the convergence conditions stated earlier in Sec. IV are met but it may be overly stringent, especially when  $ka = 1000$ . With  $ka = 100$ , consider the convergence illustrated in Figs. 5-7 and the results  $\eta_\infty - \eta_{16} \approx 0.9, 1.1, 1.2$ , and 1.2 for  $M = 0.94, 0.8, 0.6$ , and 0.5 respectively; notice that for  $M = 0.94$ ,  $N = 8$  was sufficient even though  $\eta_\infty - \eta_8 \approx 3.7$ .
28. L. Levey and L. B. Felsen, "On incomplete Airy functions and their application to diffraction problems," Radio Sci. 4, 959-969 (1969).
29. P. L. Marston and D. S. Langley, "Strong backscattering and depolarization from bubbles and glass spheres in water (abstract)," J. Opt. Soc. Am. 72, xxx (1982) at press.
30. G. E. Duvall, "24 kc echoes from a 3-foot sphere," UCDWR Report IR A32 (University of California, San Diego, 1944).

31. R. H. Wallace, H. V. Hillery, G. R. Barnard, B. M. Marks, and C. M. McKinney, "Experimental investigation of several passive sonar targets," *J. Acoust. Soc. Am.* 57, 862-869 (1975).
32. D. L. Polda, "Target strength of focussed liquid-filled spherical reflectors," *J. Acoust. Soc. Am.* 49, 1596-1599 (1971).
33. R. Hickling, "Analysis of echoes from a hollow metallic sphere in water," *J. Acoust. Soc. Am.* 36, 1124-1137 (1964); K. J. Diercks and R. Hickling, "Echoes from hollow aluminum spheres in water," *ibid.* 41, 380-393 (1967).
34. C. L. Brockman and N. G. Alexopoulos, "Geometrical optics of inhomogeneous particles: glory ray and rainbow revisited," *Appl. Opt.* 16, 166-174 (1977).

TABLE I. Model results for form function moduli<sup>a</sup> when  $\rho_1 = \rho_0$ .

M	ka	g <sub>n</sub> (γ = 0)			f <sub>n</sub> (γ = 0)			
		8	16	0	2	4		
0.94	100	4.0 E-2	1.0 E-2	7.1 E-4	1.1 E-4	3.1 E-2	2.7 E-2	9.1 E-6
0.94	1000	1.3 E-1	3.2 E-2	2.2 E-3	3.6 E-4	3.1 E-2	2.7 E-2	9.1 E-6
0.60	100	5.2 E-1	3.1 E-1	7.4 E-2	1.8 E-2	2.5 E-1	1.0 E-1	2.6 E-3
0.60	1000	1.65	9.7 E-1	2.3 E-1	5.7 E-2	2.5 E-1	1.0 E-1	2.6 E-3

<sup>a</sup>E-1 and E-2 are factors of 10<sup>-1</sup> and 10<sup>-2</sup> respectively, etc.

TABLE II. Focal circle parameters for  $M = 0.94$  (upper group) and  $0.6$  (lower group).  $B(b_n)$  is shown for the case  $\rho_1 = \rho_0$ .

n	$\theta_n$ (deg)	$b_n/a$	$\alpha_n/a$	$q_n$	$E_n$	$B(b_n)$
3	40.24	0.646	1.162	7.2	1.30	3.0 E-3
4	53.08	0.800	1.078	13.9	1.12	-9.1 E-4
8	65.62	0.911	1.016	65.1	0.57	-1.2 E-4
16	68.91	0.933	1.004	277.1	0.28	-4.0 E-5
3	21.20	0.362	1.096	11.4	0.56	9.3 E-2
4	28.24	0.473	1.052	20.4	0.54	-5.7 E-2
8	34.76	0.570	1.012	84.2	0.31	-2.3 E-2
16	36.33	0.593	1.003	340.3	0.16	-1.1 E-2

TABLE III. Exact and axial form function moduli at  $\gamma = 0$  for selected  $M > 1$  when  $\rho_1 = \rho_0$ .

M	$ f_e(ka = 100) $	$ f_e(ka = 1000) $	$ f_0 $	$ f_2 $
$M'_4$	2.57	7.12	0.042	0.051
1.10	1.97	1.99	0.048	0.058
$M'_3$	6.50	19.60	0.083	0.118
1.25	1.39	0.26	0.111	0.183

**Figure Captions**

Fig. 1. Backscattered rays from a sphere with  $M = 0.6$ . The center of the sphere is C and the figure may be rotated about the CC' axis.

Fig. 2. Path of a ray (dashed line) as it leaves the sphere.

Fig. 3. Angles and distances needed to describe a point  $(x', y')$  in the exit plane and the observation point Q. The z axis is the extension (toward the source) of the CC' axis.

Fig. 4. Distances needed to describe the phase of the reflected wave.

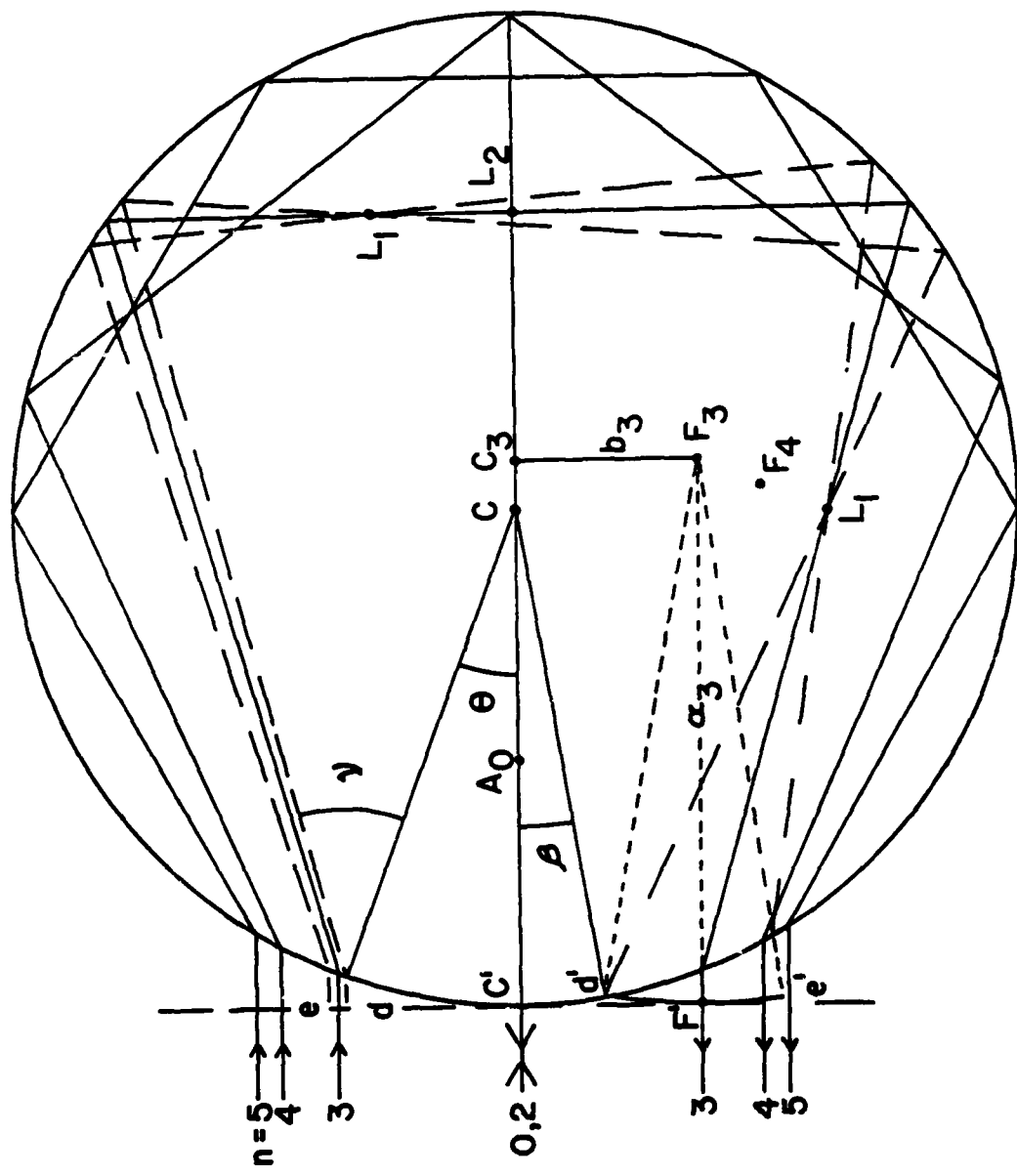
Fig. 5. Comparison of exact and model form functions of spheres with  $M = 0.94$ . The curves labeled N give  $|f|$  from Eq. (36) evaluated with the indicated N. In (a), the model result (dotted curve) is nearly identical to the exact result (solid curve).

Fig. 6. Comparison as in Fig. 5 but with  $M = 0.6$ .

Fig. 7. Comparisons as in Fig. 5 but for (a)  $M = 0.8$ , and (b)  $M = 0.5$ , with  $ka = 100$  in both cases.

Fig. 8. Combined rainbow-glory ray for a sphere with  $M = M'_3$  of Eq. (4). The distance scales in the sketch of the cubic wavefront have been enlarged for enhanced visibility.

Fig. 9. Comparison of exact (solid curves) and modeled (dashed curves) form functions of spheres with  $ka = 1000$  (upper group) and 100 (lower group). The model results are from Eq. (42) which describes only the rainbow-enhanced glory ray. The ray is the  $n = 3$  ray in Fig. 8 which has  $b_3 \approx 0.9752$  a.



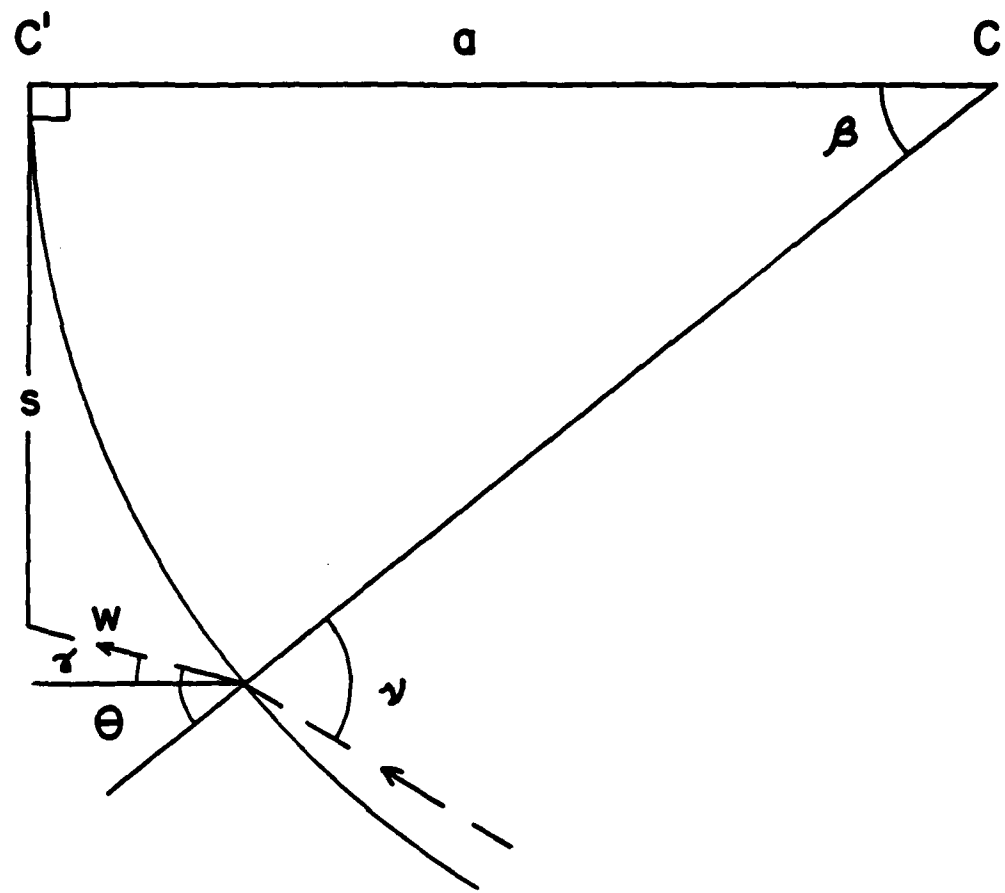


Fig. 2

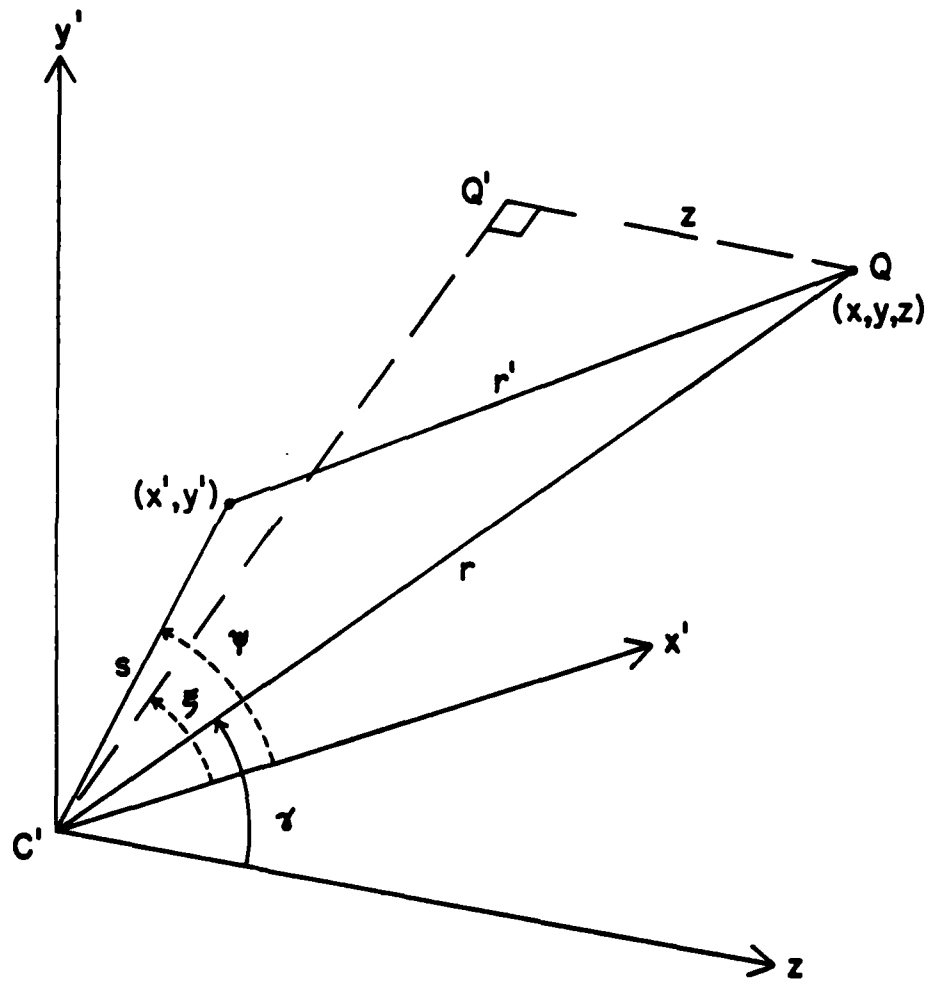


Fig. 3

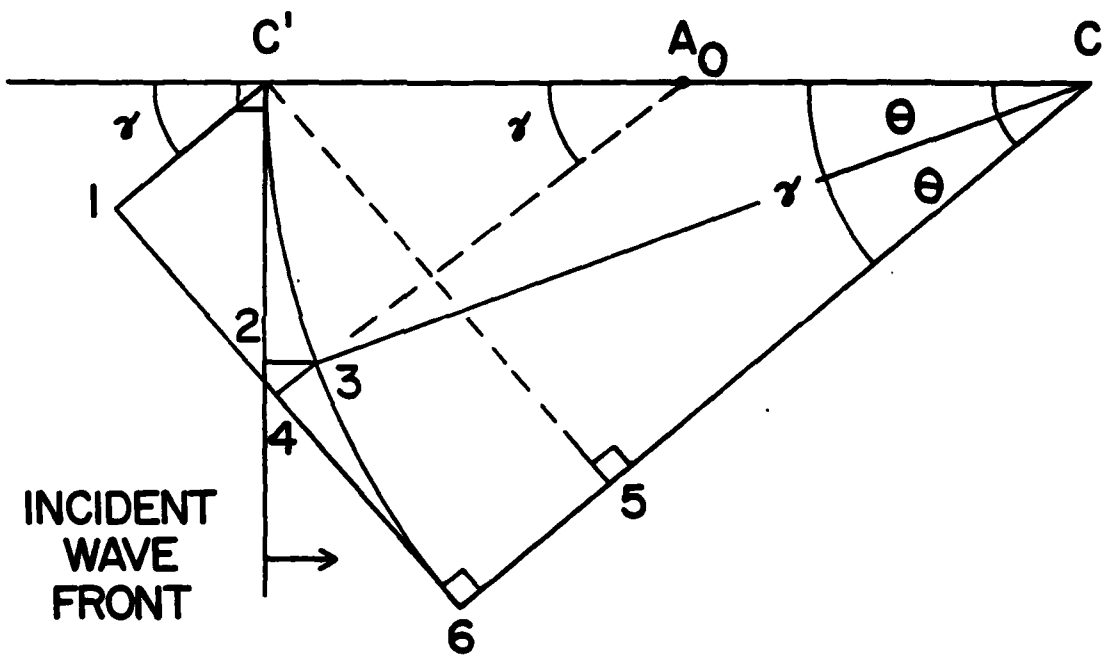


Fig. 4

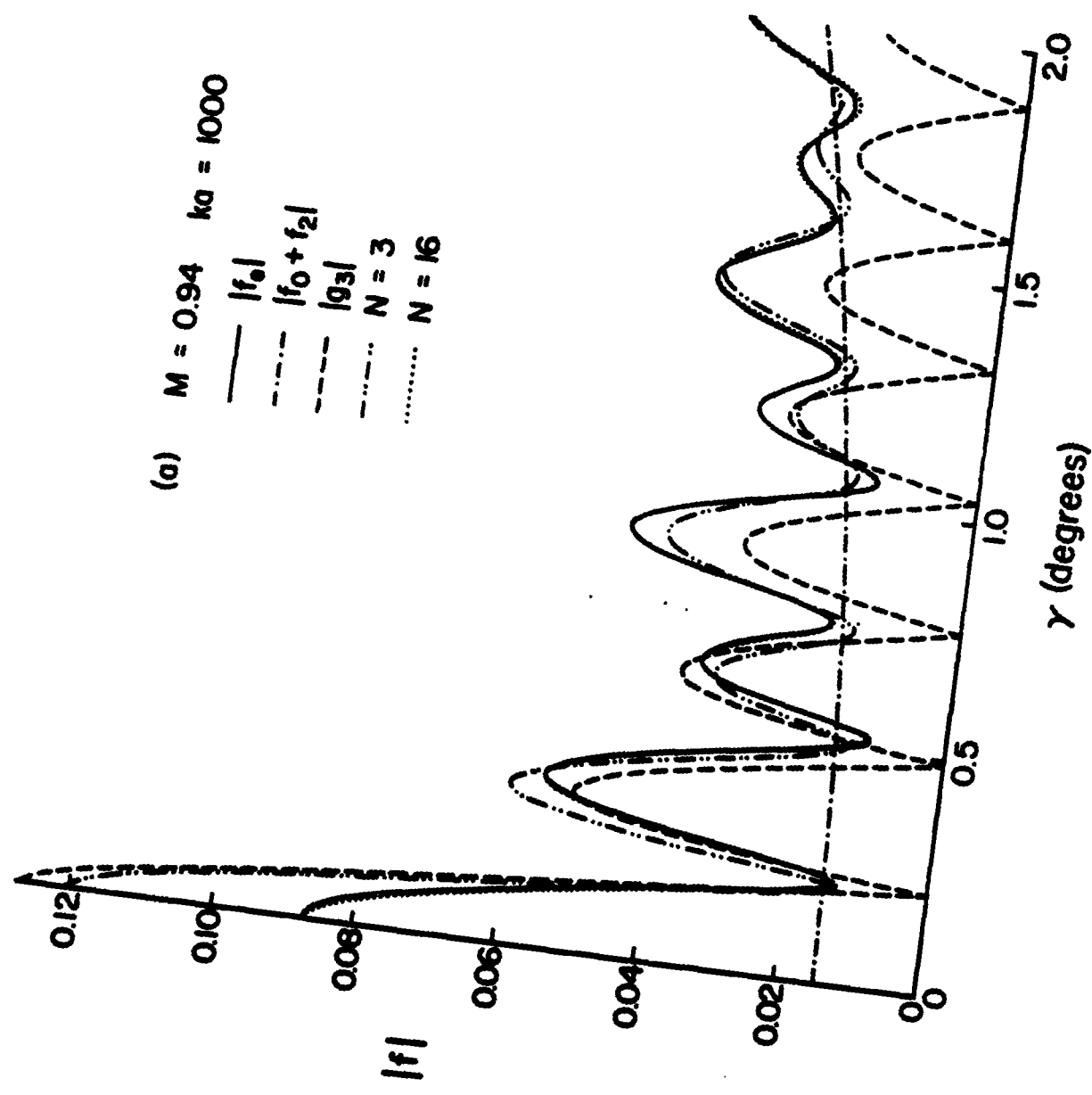


Fig. 5a

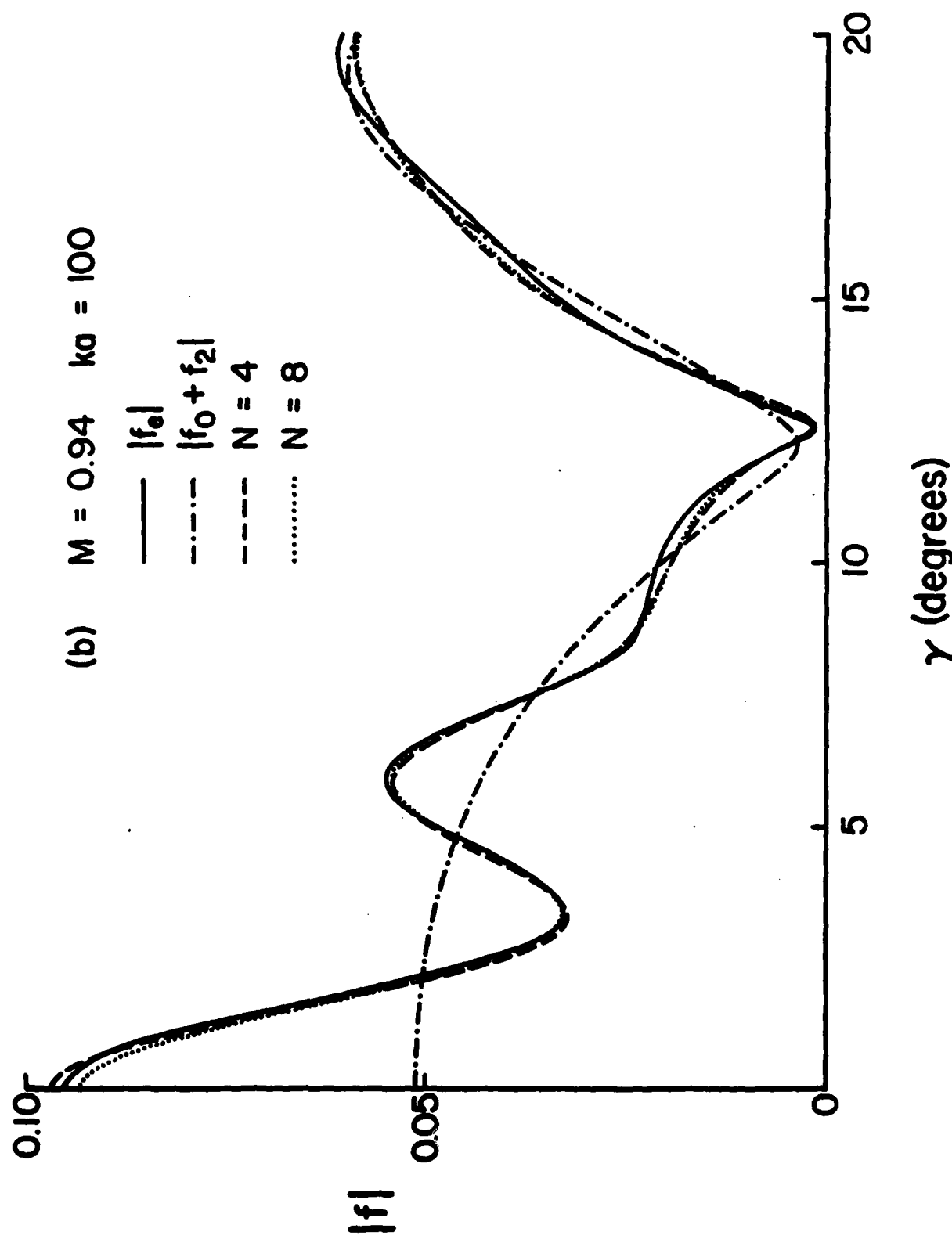


Fig. 5b

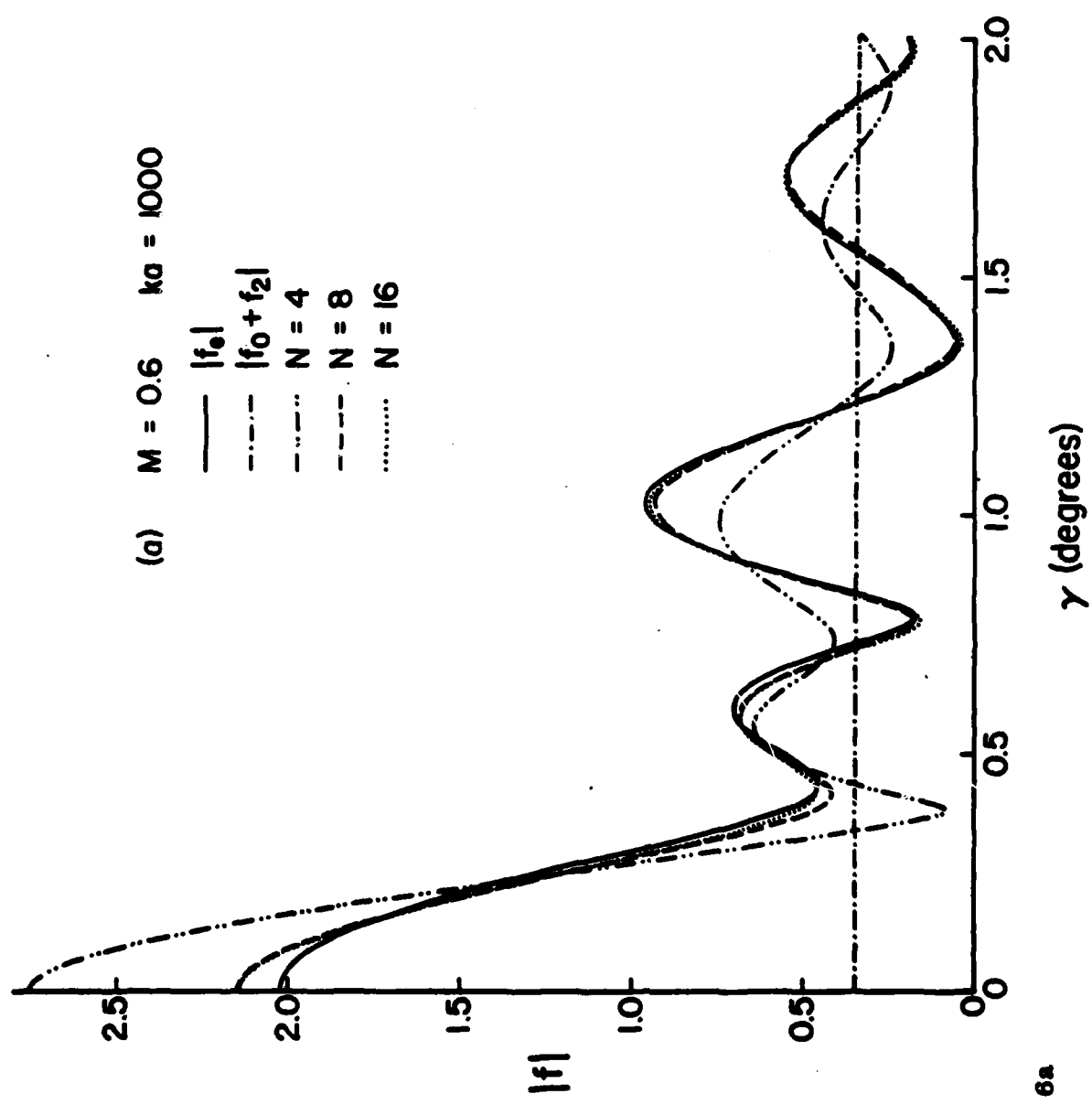


FIG. 6a

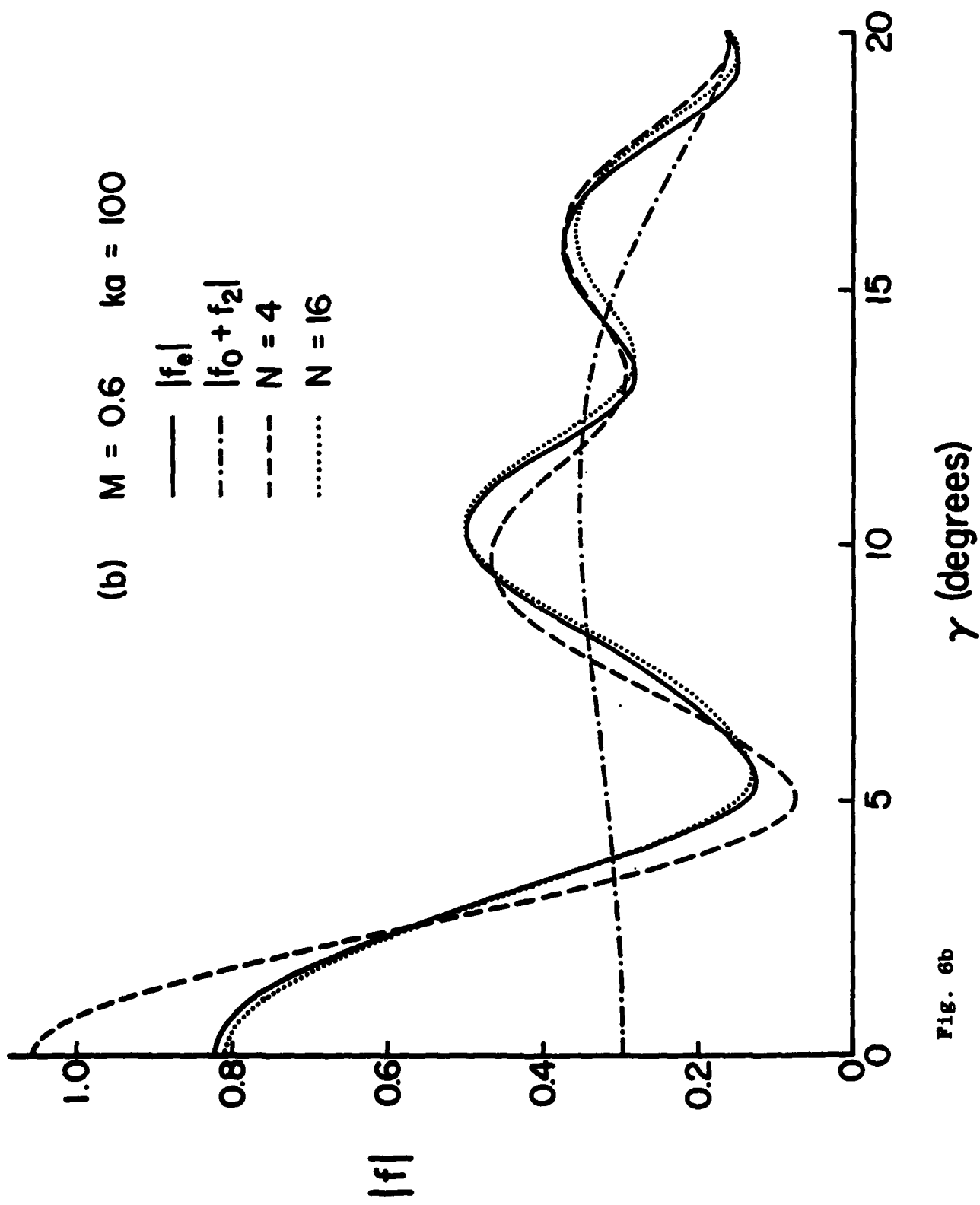


FIG. 6b

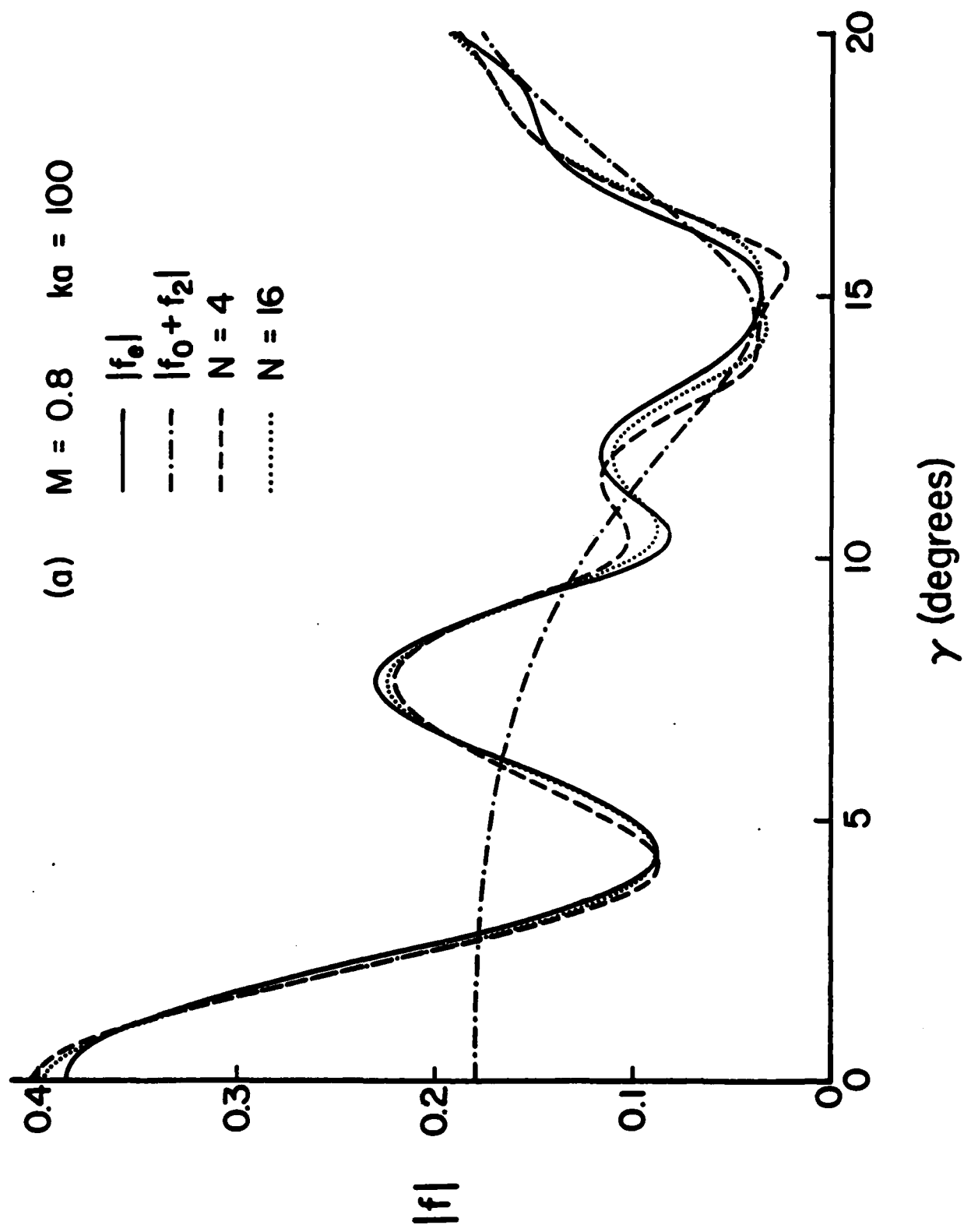


Fig. 7a

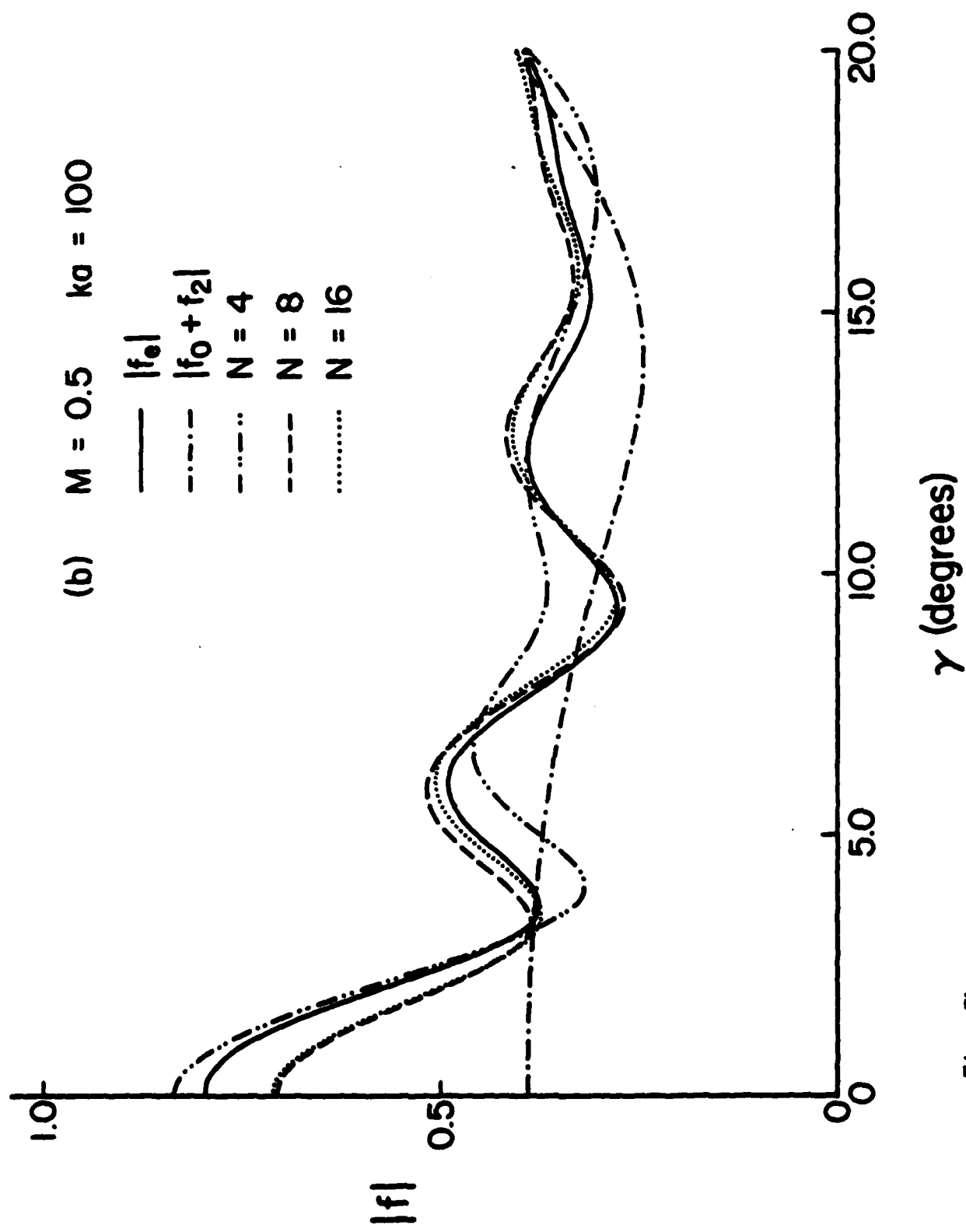


FIG. 7b

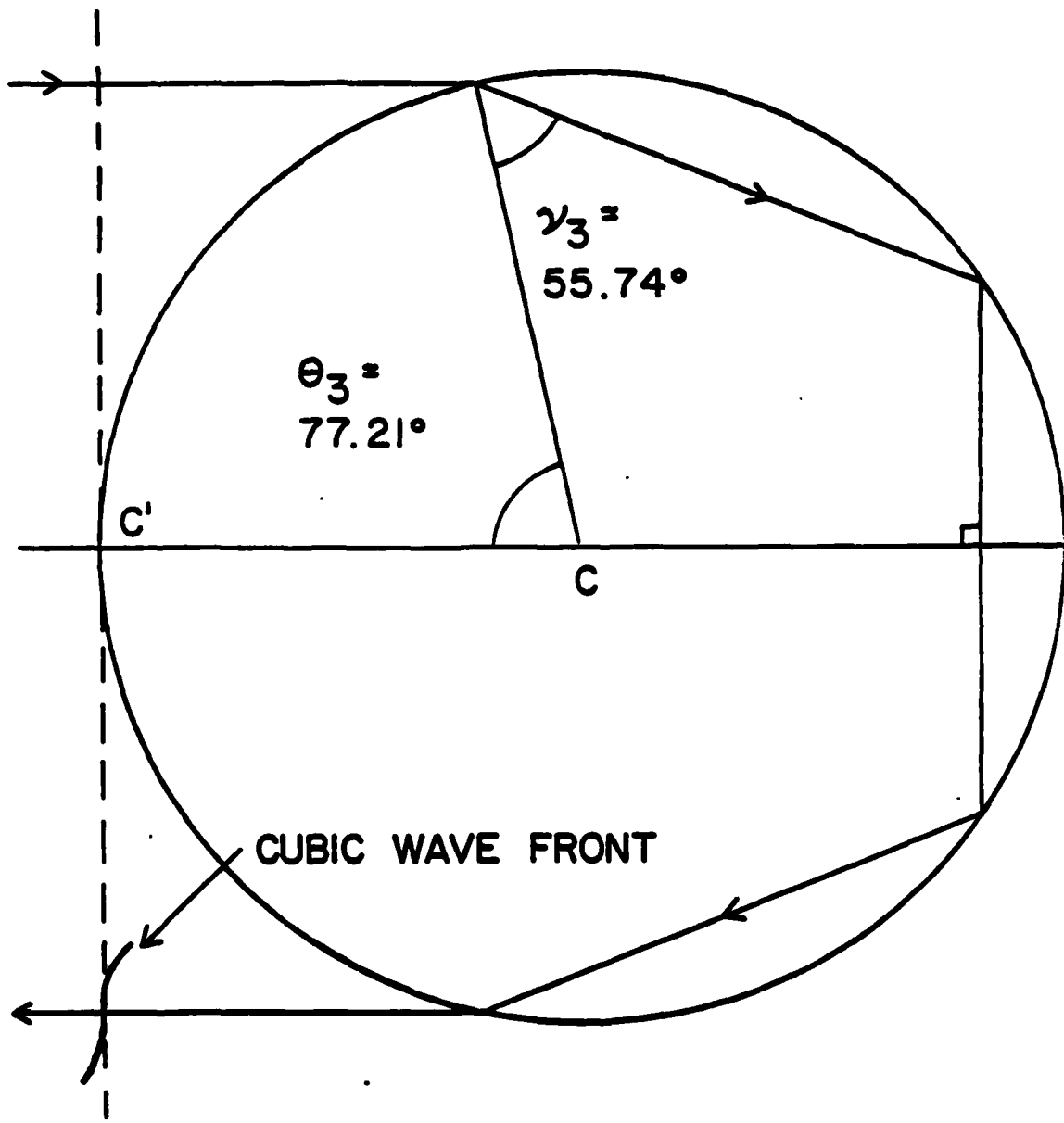


Fig. 8

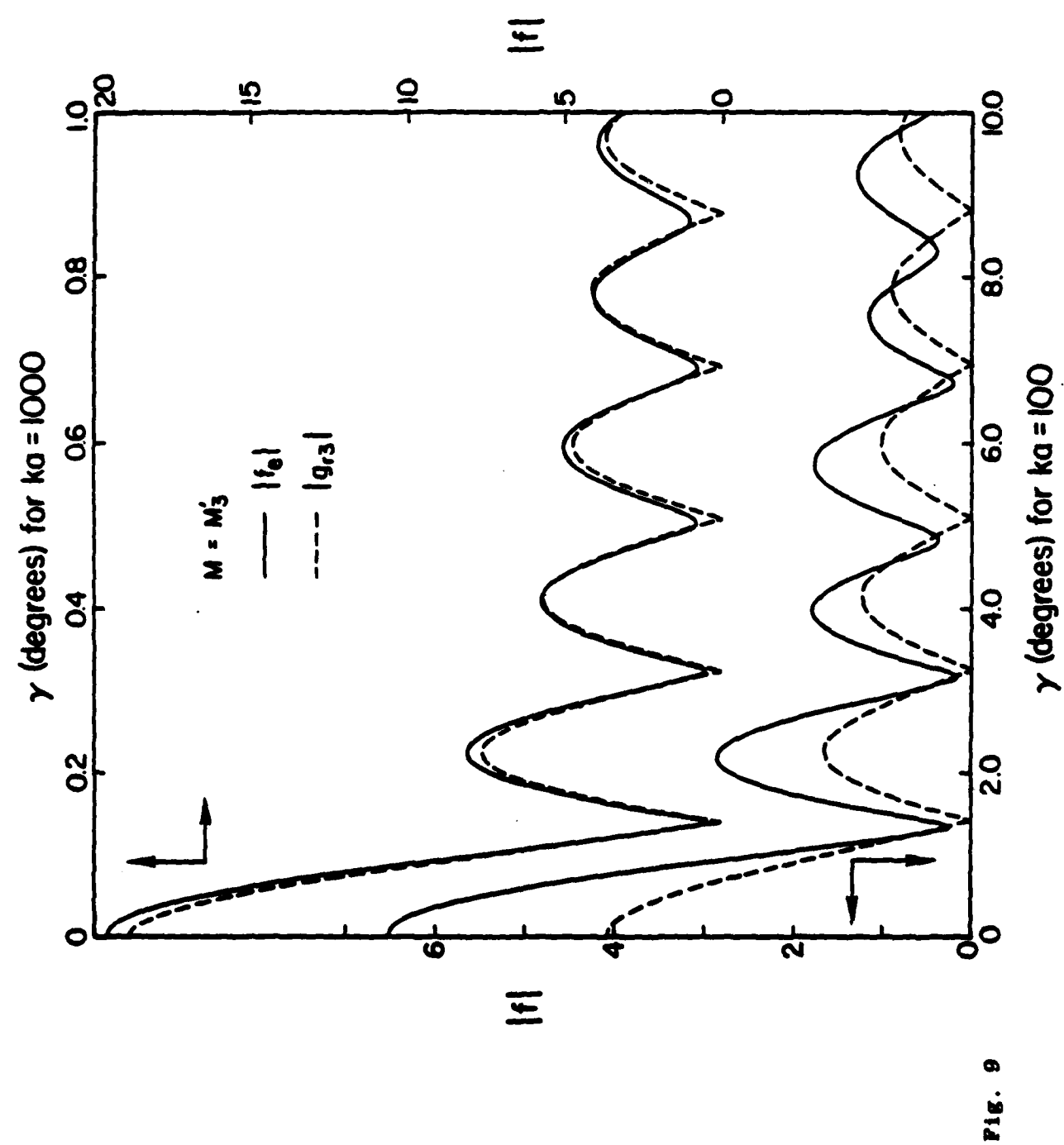


FIG. 9

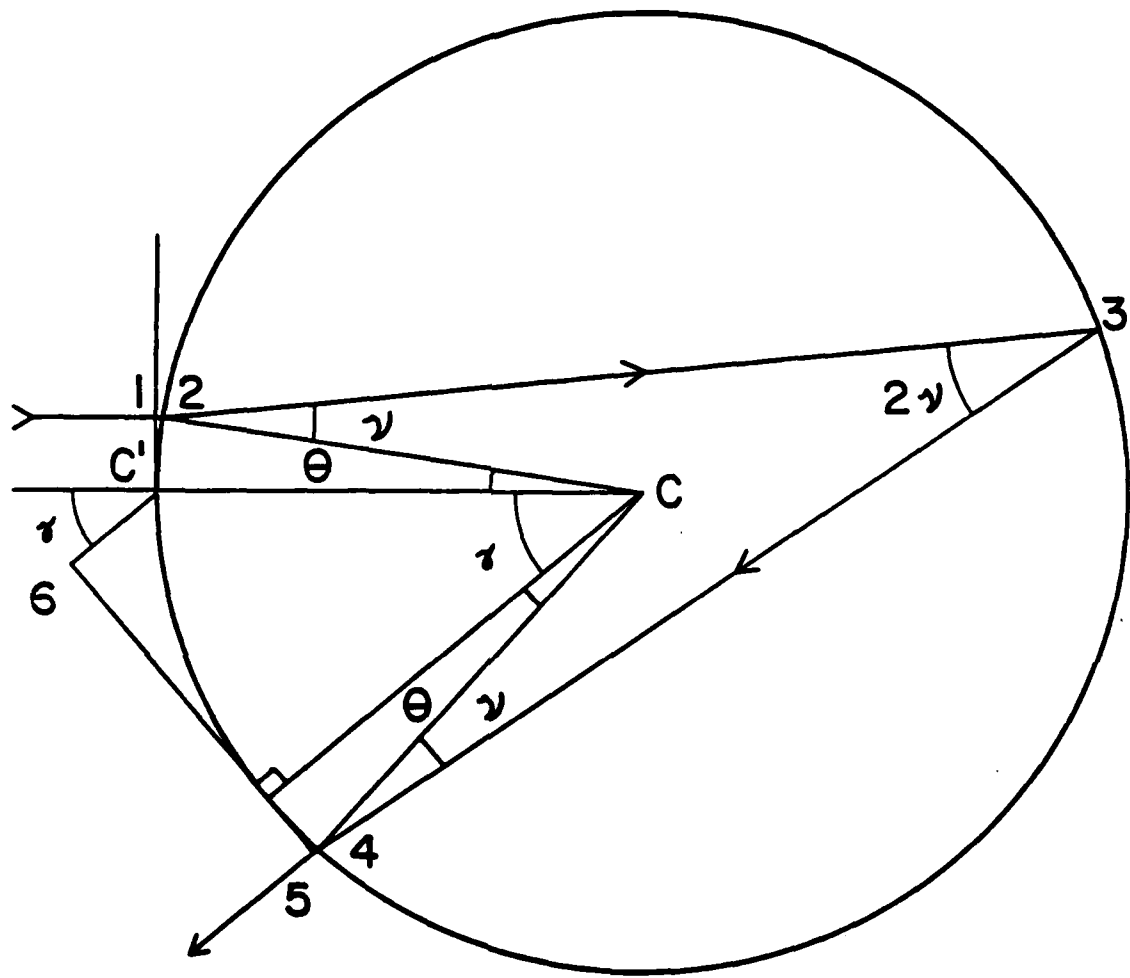


Fig. C-1. Distances and angles needed to describe the scattering due to the single bounce "axial ray."  $\theta$  is the ray's angle of incidence. The refraction angle  $\nu$  is illustrated for the case  $M = 0.6$ .

Submitted to the 104th Meeting of the Acoustical Society of America  
9-12 November 1982

Observation of the acoustic glory: Scattering from an elastic sphere in near backward directions. Philip L. Marston, Timothy J. B. Hanson,<sup>a)</sup> and Kevin L. Williams (Dept. of Physics, Washington State University, Pullman, WA 99164)

We have measured the scattering for small angles  $\gamma$  (relative to the backward axis) from a fused silica sphere of radius  $a \approx 52$  mm. Tone bursts in water corresponding to  $ka \approx 450$  were incident on the sphere; their short duration permitted glory and axial returns to be separated in time. The  $\gamma$  for the probe hydrophone was scanned to test a model [P. L. Marston and L. Flax, J. Acoust. Soc. Am. Suppl. 68, S81 (1980)] of diffractive effects on backward axial focusing. Observations tend to support the model as adapted to fused silica: (1) from the arrival time, the strongest echo is evidently due to the 4-chord shear glory ray; (2) its amplitude is  $\propto J_0(kbs\sin\gamma)$  where  $b$  is the calculated glory circle radius; (3) its amplitude at  $\gamma = 0$ , though slightly smaller than predicted, exceeds that of the first axial reflection; and (4) the times, amplitudes, and  $\gamma$  dependences of other echos are correlated to predictions. The first null of the strongest echo occurs at  $\gamma \approx 1^\circ$ . Consequently, we demonstrate for the first time the diffraction limited backward focusing of echos from a sphere. [Work supported by ONR. Marston is an Alfred P. Sloan Research Fellow]

<sup>a)</sup>Present address: Defense Systems Division, Honeywell Inc., Hopkins, MN 55343

Technical Committee: Physical Acoustics

Subject Classification numbers: 43.20.Fn, 43.20.Px, 43.35.Zc

Telephone Number: (509) 335-5343 (P. L. Marston)

February 1961

REPORTS DISTRIBUTION LIST FOR OUR PHYSICS PROGRAM (DIVISION) OFFICE  
UNCLASSIFIED CONTRACTS

Director Defense Advanced Research Projects Agency	3 copies	1 copy
Attn: Technical Library 1100 Wilson Blvd. Arlington, Virginia 22209		
Office of Naval Research Physics Division Office (Code 412) 800 North Quincy Street Arlington, Virginia 22217	3 copies	3 copies
Office of Naval Research Director, Technology (Code 200) 800 North Quincy Street Arlington, Virginia 22217	1 copy	1 copy
Naval Research Laboratory Department of the Navy Attn: Technical Library Washington, DC 20375	3 copies	1 copy
Office of the Director of Defense Research and Engineering Information Office Library Branch The Pentagon Washington, DC 20301	1 copy	1 copy
U. S. Army Research Office Box 1221 Research Triangle Park North Carolina 27709	2 copies	1 copy
Defense Technical Information Center Cameron Station Alexandria, Virginia 22316	12 copies	1 copy
Director, National Bureau of Standards Attn: Technical Library Washington, DC 20234	1 copy	1 copy
Commanding Officer Office of Naval Research Western Regional Office 1130 East Green Street Pasadena, California 91101	3 copies	1 copy
Commanding Officer Office of Naval Research Eastern/Central Regional Office 666 Summer Street Boston, Massachusetts 02210	3 copies	1 copy
Director U. S. Army Engineering Research and Development Laboratories Attn: Technical Documents Center Fort Belvoir, Virginia 22060	3 copies	3 copies
ODDRAE Advisory Group on Electron Devices 201 Varick Street New York, New York 10013		
Air Force Office of Scientific Research Department of the Air Force Bolling AFB, D. C. 20332	1 copy	1 copy
Air Force Weapons Laboratory Technical Library Albuquerque, New Mexico 87117	1 copy	1 copy
Air Force Avionics Laboratory Air Force Systems Command Technical Library Wright-Patterson Air Force Base Dayton, Ohio 45433	1 copy	1 copy
Lawrence Livermore Laboratory Attn: Dr. V. F. Krupke University of California P.O. Box 608 Livermore, California 94550	1 copy	1 copy
Naval Air Development Center Technical Library 2800 Powder Mill Road Adelphi, Maryland 20783	1 copy	1 copy
Naval Diamond Laboratories Technical Library Johnsville Warminster, Pennsylvania 18974	1 copy	1 copy
Naval Air Development Center Attn: Technical Library Johnsville Warminster, Pennsylvania 18974	1 copy	1 copy
Naval Weapons Center Technical Library (Code 753) China Lake, California 93555	1 copy	1 copy
Naval Training Equipment Center Technical Library Orlando, Florida 32813	1 copy	1 copy
Naval Underwater Systems Center Technical Center New London, Connecticut 06320	1 copy	1 copy

Commandant of the Marine Corps  
Scientific Advisor (Code 80-1)  
Washington, DC 20380

Naval Ordnance Station  
Technical Library  
Indian Head, Maryland 20650

Naval Postgraduate School  
Technical Library (Code 0212)  
Monterey, California 93940

Naval Missile Center  
Technical Library (Code 5632.2)  
Point Mugu, California 93010

Naval Ordnance Station  
Technical Library  
Louisville, Kentucky 40214

Commanding Officer  
Naval Ocean Research & Development Activity  
NSTL Station, Mississippi 39529

Naval Explosive Ordnance Disposal Facility  
Technical Library  
Indian Head, Maryland 20640

Naval Ocean Systems Center  
Technical Library  
San Diego, California 92152

Naval Surface Weapons Center  
Technical Library  
Silver Spring, Maryland 20910

Naval Ship Research and Development Center  
Central Library (Code 142 and 143)  
Bethesda, Maryland 20885

Naval Avionics Facility  
Technical Library  
Indianapolis, Indiana 46218

1 copy

Dr. L. Flax  
Code 791  
Naval Coastal Systems Center  
Panama City, FL 32407

1 copy

Don Rottier  
Code 791  
Naval Undersea Warfare Eng. Station  
Keyport, WA 98345

1 copy

Dr. M. Medwin  
Department of Physics  
U.S. Naval Postgraduate School  
Monterey, CA 93940

1 copy

Dr. G. C. Gauthier  
Naval Surface Weapons Center  
R-31, White Oak  
Silver Spring, MD 20910

1 copy

Dr. Robert E. Apfel  
Mason Laboratory  
Yale University  
P.O. Box 2159  
New Haven, CT 06520

1 copy

Dr. D. T. Blackstock  
Applied Research Laboratory  
University of Texas  
Austin, TX 78712

1 copy

Dr. Lawrence A. Crum  
Department of Physics  
University of Mississippi  
University, MS 38677

1 copy

Dr. Joseph B. Keller  
Department of Mathematics  
Stanford University  
Stanford, CA 94305

1 copy

Dr. Taylor Wang  
Jet Propulsion Laboratory  
4800 Oak Grove  
Pasadena, CA 91103

Dr. M. Uherall  
Department of Physics  
Catholic University  
Washington, D.C. 20064

Dr. L. R. Dragonette, Code 5134  
Naval Research Laboratory  
Washington, D.C. 20375

Dr. D. L. Polda  
Naval Coastal Systems Center  
Panama City, FL 32407

Dr. H. Hedin  
Department of Physics  
U.S. Naval Postgraduate School  
Monterey, CA 93940

Dr. C. Gauthier  
Naval Surface Weapons Center  
R-31, White Oak  
Silver Spring, MD 20910

Dr. Robert E. Apfel  
Mason Laboratory  
Yale University  
P.O. Box 2159  
New Haven, CT 06520

Dr. D. T. Blackstock  
Applied Research Laboratory  
University of Texas  
Austin, TX 78712

Dr. Lawrence A. Crum  
Department of Physics  
University of Mississippi  
University, MS 38677

Dr. Joseph B. Keller  
Department of Mathematics  
Stanford University  
Stanford, CA 94305

Dr. Taylor Wang  
Jet Propulsion Laboratory  
4800 Oak Grove  
Pasadena, CA 91103

Dr. Akira Ishimaru  
Dept. of Electrical Engineering  
University of Washington  
Seattle, WA 98195

